DOKUZ EYLÜL UNIVERSITY
GRADUATE SCHOOL OF NATURAL AND APPLIED SCIENCES

MATHEMATICAL MODELING OF ELECTROCHEMICAL HYDROGEN COMPRESSORS

by
Cemil KUZU

July, 2024
İZMİR

MATHEMATICAL MODELING OF ELECTROCHEMICAL HYDROGEN COMPRESSORS

A Thesis Submitted to the
Graduate School of Natural and Applied Sciences of Dokuz Eylül University
In Partial Fulfillment of the Requirements for Master of Science in
Department of Mechanical Engineering, Thermodynamics Program

by
Cemil KUZU

July, 2024
İZMİR

M.Sc THESIS EXAMINATION RESULT FORM

We have read the thesis entitled **"MATHEMATICAL MODELING OF ELECTROCHEMICAL HYDROGEN COMPRESSORS"** completed by **CEMİL KUZU** under supervision of **PROF. DR. CAN ÖZGÜR ÇOLPAN** and **PROF. DR. YILSER DEVRİM** and we certify that in our opinion it is fully adequate, in scope and in quality, as a thesis for the degree of Master of Science.

Prof.Dr. Can Özgür ÇOLPAN

Supervisor

Prof.Dr.Erdal ÇETKİN

Jury Member

Prof.Dr. Aytunç EREK

Jury Member

Prof. Dr. Okan FISTIKOĞLU

Director

Graduate School of Natural and Applied Sciences

ACKNOWLEDGMENT

I would like to extend my appreciation to my supervisor Prof. Dr. Can Özgür ÇOLPAN for his invaluable guidance, counsel, motivation, support, and profound insights throughout the entirety of the research process. His steadfast presence during every challenge encountered in this journey, coupled with his unwavering support and guidance, has been invaluable. I am truly grateful for the wealth of experiences he shared and the lessons he imparted, shaping my understanding, and enhancing my capabilities.

I express my sincere gratitude to my co-supervisor who contributed to enriching the thesis with her valuable comment, Prof. Dr. Yılser DEVRİM. I am deeply appreciative of her unwavering support for the experimental studies and the opportunities she provided, contributing immensely to the overall quality and depth of this work.

I wish to express my special thanks to my dear friends Tacettin DİŞLİ, Can AKÇALI, Sera Ayten ÇETİNKAYA, Berk BAŞARAN, Beyza Nisan DURSUN, and Gizem Nur BULANIK DURMUŞ for their valuable contributions in this study.

The author thanks to the Scientific and Technological Research Council of Turkey (TÜBİTAK) 1001 (Grant number: 219M333) Project.

Finally, I would like to express my most special thanks to my parents Sami KUZU and Selma KUZU, my siblings, and my dearest friend İzel BEREKETOĞLU, who made me feel their support and trust throughout my life.

Cemil KUZU

MATHEMATICAL MODELING OF ELECTROCHEMICAL HYDROGEN COMPRESSORS

ABSTRACT

In this study, numerical studies on the performance of an electrochemical hydrogen compressor operating at high temperatures are presented. First, a semi-empirical mathematical model was created to examine the performance of the cell under different temperatures to investigate the optimum operating temperature value of the ECHC cell. As a result of these studies, the polarization curves of the ECHC cell in the case of pure hydrogen gas feeding and mixed gas feeding are presented graphically. The operating temperature value with the highest efficiency was observed as 160°C. After determining the operating temperature as 160°C, the current values drawn by the cell from the power supply over time at constant cell voltage values are presented as a Current-Time graph. To examine the pressurization performance of the ECHC cell, separate numerical models were created with single-cell and 5-cell stacked cell designs. Using the Current-Time graph created by the ECHC cell under different constant voltage values as input, the forward and backward hydrogen molar flow rate was calculated for each cell voltage. According to the obtained molar flow rate values, the pressure values obtained for each cell voltage were obtained using the ideal gas law and presented through graphs. In the single-cell ECHC cell, 60 bar levels were reached after 2500 seconds at a constant cell voltage of 1.5 V. In the 5-cell stacked model design, it has been observed design reaches 60 bar shorter time than the single-cell model.

Keywords: High-Temperature ECHC, PBI-Membrane, mathematical model, back-diffusion, stack level ECHC

ELEKTROKİMYASAL HİDROJEN KOMPRESÖRLERİNİN MATEMATİKSEL MODELLEMESİ

ÖZ

Bu çalışmada, yüksek sıcaklıkta çalışan bir elektrokimyasal hidrojen kompresörünün performansına ilişkin sayısal araştırmalar sunulmaktadır. İlk olarak EKHK hücresinin optimum çalışma sıcaklık değerinin araştırılması için farklı sıcaklıklar altında hücrenin performansını incelemek amacıyla yarı deneysel bir matematiksel model oluşturulmuştur. Bu çalışmalar sonucunda hücrenin saf hidrojen gazı beslemesi ve karışım gazı beslemesi durumunda EKHK hücresinin polarizasyon eğrileri grafiklerle sunulmuştur. Verimin en yüksek olduğu çalışma sıcaklığı değeri 160°C olarak gözlemlenmiştir. Çalışma sıcaklığının 160°C olarak belirlenmesinden sonra hücrenin sabit tutulan hücre voltajı değerlerinde zamanla güç kaynağından çektiği akım değerleri Akım-Zaman grafiği şeklinde sunulmuştur. EKHK hücresinin basınçlandırma performansını incelemek adına tek hücre ve 5 hücreli yığın hücre tasarımlı olacak şekilde ayrı ayrı sayısal modeller oluşturulmuştur. Farklı sabit voltaj değerleri altında EKHK hücresinin oluşturduğu Akım-Zaman grafiği girdi olarak kullanılarak, her hücre voltajı için ileri ve geri yönlü hidrojen akısı hesaplanmıştır. Elde edilen akı değerlerine göre ideal gaz yasası kullanılarak her bir hücre voltajı için elde edilen basınç değerleri elde edilmiş ve grafikler aracılığıyla sunulmuştur. Tek hücreli EKHK hücresinde 1.5 V sabit hücre voltajında 2500 saniye sonunda 60 bar mertebelerine ulaşılmıştır. 5 hücreli yığın model tasarımında ise tek hücreli modele kıyasla daha kısa sürede 60 bar seviyesine ulaştığı gözlemlenmiştir.

Anahtar kelimeler: Yüksek Sıcaklık EKHK, PBI-Membran, matematiksel model, geri difüzyon, yığın model EKHK tasarımı

CONTENTS

Page

M.Sc THESIS EXAMINATION RESULT FORM ii
ACKNOWLEDGMENT iii
ABSTRACT iv
ÖZ v
CONTENTS vi
LIST OF FIGURES viii
LIST OF TABLES xii
ABBREVIATIONS xiii

CHAPTER ONE INTRODUCTION 1

1.1 Introduction 1
1.2 Motivation 3
1.3 Objective 3
1.4 Thesis Outline 4

CHAPTER TWO BACKGROUND AND LITERATURE SURVEY 5

2.1 Hydrogen Compression Methods 5
2.1.1 Mechanical Compressors 6
2.1.2 Non-mechanical Compressors 7
2.2 Electrochemical Hydrogen Compressors 9
2.2.1 Membranes 10
2.2.2 Catalyst 11
2.2.3 Gas Diffusion Layer 11
2.2.4 Bipolar plates and end plates 12
2.3 Literature Survey 14

CHAPTER THREE MATHEMATICAL MODEL 19

3.1 Working Principle of ECHC 19

3.1.1 High-Temperature ECHC Semi-Experimental Mathematical Model Development 20
3.1.2 Investigating Back Diffusion's Effect on a Single Cell ECHC Performance Using Mathematical Modeling 22
3.1.3 Investigating Back Diffusion's Effect on a Stack Level ECHC Performance Using Mathematical Modeling 26
3.2 Calibration of the Modeling Parameters using PSO Algorithm 30
3.3 Model Verification 33
3.4 Experimental Studies 36

CHAPTER FOUR RESULTS AND DISCUSSION 43

4.1 Operation with Pure H_2 Feeding 43
4.2 Operation with Feeding Reformate Gas Mixtures 44
4.3 Comparison and Interpretation of the Efficiencies of the Results Obtained at Different Ratios of Mixing Gas 47
4.4 Effect of Back Diffusion at Constant Cell Voltage (Single Cell) 47
4.4.1 Investigation of the Change of Forward and Backward H_2 Molar flow rate with Time at Different Cell Voltage Values 48
4.4.2 Investigation of the Change of the Amount of H_2 Transferred with Time at Different Cell Voltage Values 53
4.4.3 Investigation of Pressure Values Obtained at Different Cell Voltage Values and Validation with Experimental Data 57
4.4.4 Investigation of Efficiency of ECHC Cell at Different Cell Voltages 61
4.5 Investigation of the 5-cell Stack through Modeling 66
4.6 Characterizing the ECHC Cell's Polarization Curve through Parameter Calibration with the PSO Algorithm 67

CHAPTER FIVE 69

REFERENCES 71

LIST OF FIGURES

Page

Figure 2. 1 Schematic representation of mechanical and non-mechanical hydrogen compressors (Durmus et al., 2021) 5
Figure 2. 2 ECHC components, Bulanık Durmuş et al., (2024) 10
Figure 2. 3 Diagram showing the plastic forming techniques used to create BPPs made of stainless steel (a)stamping (b) hydroforming (c) rubber pad forming (d) direct roll forming Leng et al., (2020) 13
Figure 3. 1 Schematic view of ECHC working principle 19
Figure 3. 2 Schematic representation of the series-connected stack ECHC model 27
Figure 3. 3 Schematic representation of the control volumes of the series connected stack ECHC model 27
Figure 3. 4 Change of forward and backward H_2 molar flow rate over time at a constant cell voltage of 0.075 V 34
Figure 3. 5 Change of forward and backward transferred H_2 molar flow rate over time at a constant cell voltage of 0.075 V 35
Figure 3. 6 Change of cathode pressure with time at a constant cell voltage of 0.075 V 35
Figure 3. 7 Variation of ECHC cell current, voltage, and cell efficiency with time at a constant cell voltage of 0.075 V 36
Figure 3. 8 PBI membrane preparation steps, Bulanık Durmuş et al., (2024) 37
Figure 3. 9 GDE preparation steps, Bulanık Durmuş et al., (2024) 38
Figure 3. 10 MEA preparation steps, Bulanık Durmuş et al., (2024) 38
Figure 3. 11 Single-cell HT-ECHC, Bulanık Durmuş et al., (2024) 39
Figure 3. 12 Stack level (5 cell) HT-ECHC, Bulanık Durmuş et al., (2024) 39
Figure 3. 13 The assembled HT-ECHC single cell and stack, Bulanık Durmuş et al., (2024) 40
Figure 3. 14 HT-ECHC purification test setup flow diagram, Bulanık Durmuş et al., (2024) 41
Figure 3. 15 HT-ECHC performance test system, Bulanık Durmuş et al., (2024) 41

Figure 4. 1 Experimental and modelling results of pure H_2 gas between 140°C-180°C temperatures 44
Figure 4. 2 Experimental and modeling results of H_2/CO_2 (0.75:0.25) gas mixture between 140°C-180°C temperatures 45
Figure 4. 3 Experimental and modeling results of $H_2/CO_2/CO$ (0.73:0.26:0.02) gas mixture between 140°C-180°C temperatures 46
Figure 4. 4 Experimental and modeling results of H_2/CO (0.95:0.05) gas mixture between 140°C-180°C temperatures 46
Figure 4. 5 Experimental and modeling results of H_2/CO (0.97:0.03) gas mixture between 140°C-180°C temperatures 47
Figure 4. 6 Variation of current with time at different operating cell voltages 48
Figure 4. 7 Change of forward and backward H_2 molar flow rate over time at a constant cell voltage of 0.1 V 49
Figure 4. 8 Change of forward and backward H_2 molar flow ratees over time at a constant cell voltage of 0.2 V 50
Figure 4. 9 Change of forward and backward H_2 molar flow rate over time at a constant cell voltage of 0.4 V 50
Figure 4. 10 Change of forward and backward H_2 molar flow rate over time at a constant cell voltage of 0.6 V 51
Figure 4. 11 Change of forward and backward H_2 molar flow rate over time at a constant cell voltage of 0.8 V 52
Figure 4. 12 Change of forward and backward H_2 molar flow rate over time at a constant cell voltage of 1 V 52
Figure 4. 13 Change of forward and backward H_2 molar flow rate over time at a constant cell voltage of 1.5 V 53
Figure 4. 14 Change of H_2 value transferred over time at 0.1 V constant cell voltage 53
Figure 4. 15 Change of H_2 value transferred over time at 0.2 V constant cell voltage 54
Figure 4. 16 Change of H_2 value transferred over time at 0.4 V constant cell voltage 55

Figure 4. 17 Change of H_2 value transferred over time at 0.6 V constant cell voltage 55
Figure 4. 18 Change of H_2 value transferred over time at 0.8 V constant cell voltage 56
Figure 4. 19 Change of H_2 value transferred over time at 1 V constant cell voltage 56
Figure 4. 20 Change of H_2 value transferred over time at 1.5 V constant cell voltage 57
Figure 4. 21 Change of cathode pressure with time at a constant cell voltage of 0.1 V 58
Figure 4. 22 Change of cathode pressure with time at a constant cell voltage of 0.2 V 58
Figure 4. 23 Change of cathode pressure with time at a constant cell voltage of 0.4 V 59
Figure 4. 24 Change of cathode pressure with time at a constant cell voltage of 0.6 V 59
Figure 4. 25 Change of cathode pressure with time at a constant cell voltage of 0.8 V 60
Figure 4. 26 Change of cathode pressure with time at a constant cell voltage of 1 V 60
Figure 4. 27 Change of cathode pressure with time at a constant cell voltage of 1.5 V 61
Figure 4. 28 Variation of ECHC cell current, voltage and cell efficiency with time at a constant cell voltage of 0.1 V 62
Figure 4. 29 Variation of ECHC cell current, voltage and cell efficiency with time at a constant cell voltage of 0.2 V 63
Figure 4. 30 Variation of ECHC cell current, voltage and cell efficiency with time at a constant cell voltage of 0.4 V 63
Figure 4. 31 Variation of ECHC cell current, voltage and cell efficiency with time at a constant cell voltage of 0.6 V 64
Figure 4. 32 Variation of ECHC cell current, voltage and cell efficiency with time at a constant cell voltage of 0.8 V 64

Figure 4. 33 Variation of ECHC cell current, voltage and cell efficiency with time at a constant cell voltage of 1 V 65
Figure 4. 34 Variation of ECHC cell current, voltage and cell efficiency with time at a constant cell voltage of 1.5 V 65
Figure 4. 35 Variation of ECHC stack level cell pressure with time at a constant cell voltage of 7.5 V and comparison with experimental data 66
Figure 4. 36 The current drawn by the cell under constant 0.1 V 67
Figure 4. 37 Current voltage curve of the cell..... 68

LIST OF TABLES

Page

Table 2. 1 Studies on the mathematical modeling of ECHC found in the literature 16

Table 3. 1 Parameters used in the analysis of the semi-empirical model (Durmuş, 2023) 21

Table 3. 2 The parameters found by using PSO algorithm. 33

ABBREVIATIONS

$P_{Cathode}$	Cathode Pressure [Pa]
P_{Anode}	Anode Pressure [Pa]
E_{Nernst}	Nernst Voltage [V]
E_{cell}	Cell Voltage
R	Universal Gas Constant [$Jmol^{-1} \cdot K^{-1}$]
T	Operating Temperature [K]
F	Faraday's Constant [$C \cdot mol^{-1}$]
I	Current [A]
$\dot{n}_f$	Forward H_2 Molar Flow Rate [mol/s]
$\dot{n}_b$	Backward H_2 Molar Flow Rate [mol/s]
$\dot{n}_n$	Net H_2 Molar Flow Rate [mol/s]
n_f	Forward Moles [mol]
n_b	Backward Moles [mol]
n_n	Net Moles [mol]
$\eta_{current}$	Current Efficiency [-]
$\eta_{voltage}$	Voltage Efficiency [-]
η_{cell}	Cell Efficiency [-]
W_{ideal}	Ideal Work [J]
W_{actual}	Actual Work [J]
D_H	Permeability Constant [$mol \cdot m^{-1} \cdot s^{-1} \cdot Pa^{-1}$]
A	Active Area [m^2]
d	Membrane Thickness [m]

V_c	Cathode Volume [m^3]
t	Time [s]

CHAPTER ONE
INTRODUCTION

1.1 Introduction

Fossil fuels are mostly used in today's globe to meet people's demands for transportation, heating, and travel, as well as to power industrial machinery. However, considering the rate of increase in the world population, the acceleration of mechanization in the industry and the fact that fossil fuels are not a sustainable energy source, it is possible to predict that humanity will seriously seek a sustainable energy source in the future Ball & Wietschel, (2009).

In addition to the inadequacy of fossil fuels, the damage they cause to the environment due to CO_2 emissions, which is one of their biggest disadvantages, and the pollution they create have pushed researchers and engineers to search for clean and sustainable alternative sources One of the most well-liked renewable energy sources that has lately gained attention is hydrogen energy, which can be attributed to its atomic structure and upper and lower calorific values. According to Yelegen N. (2014), 1 kilogram of hydrogen contains the equivalent energy as 2.1 kg of natural gas or 2.8 kg of oil, with an upper calorific value of 140.9 MJ/kg and a lower calorific value of 120.7 MJ/kg.

The physical properties of hydrogen, coupled with its potential as a applicable energy source and its capacity to contribute to climate change mitigation, have elicited global interest, prompting the involvement of nations and enterprises in this area. In September 2019, another meeting was reported in which Japan set some important targets of 10,000 hydrogen refueling stations and 10 million hydrogen-based systems and vehicles over the course of the upcoming decade Dincer, (2020). Amil & Yılmazoğlu, (2022) stated in their study that, in addition to Japan, the Netherlands aims to use 300 thousand vehicles in the market by 2030, and France aims to use 52 thousand vehicles by 2028. It is predicted that 1000 hydrogen-powered vehicles will

be put on the market by 2030 in Turkey, which is another country with a very high potential as a hydrogen source.

Although hydrogen energy has advantages such as being clean, sustainable, and highly efficient, it also has some disadvantages that should be taken into consideration. It cannot be found in pure form in nature due to its tendency to form permanent bonds due to its monoatomic structure. This means that a purification process is required to obtain hydrogen and therefore extra costs. There are certain methods followed to purify hydrogen. Among the hydrogen purification methods, Pressure Swing Adsorption, Vacuum pressure Swing Adsorption, Cryogenic Adsorption, Carbon Membrane methods are used. The most common of these methods is Pressure Swing Adsorption (PSA). With this method, 99.999% of hydrogen can be purified (Durmus et al., 2021).

Considering the pressurization aspect adds another important section when we explore the challenges associated with hydrogen use. In terms of hydrogen pressurization, it can be delineated into two primary classifications: mechanical and non-mechanical methods. Mechanical pressurization involves using mechanical devices like compressors and pneumatic systems to increase hydrogen pressure. On the other side, non-mechanical methods are processes that don't rely on mechanical parts. Non-mechanical methods often use chemical or physical phenomena to raise hydrogen pressure, such as techniques based on adsorption or utilizing high-pressure vessels with advanced materials. These methods are explained in detail in the following Section 2.1. Taking into account that hydrogen has a density of 0.00008988 g/cm^3 at 0° C and 1 atm pressure, since it has a low-density value, it will require high-volume tanks for the volume it will occupy, and this will cause extra costs (Durmus et al., 2021). One of the technologies that can overcome these two disadvantages of hydrogen is electrochemical hydrogen compressors. These advanced systems have unique features that allow them to perform both purification and compression processes in a single device. This integration highlights the potential for increased efficiency and adaptability in using hydrogen as an energy source by reducing the processes involved in hydrogen processing.

1.2 Motivation

This thesis is driven by several key motivations, primarily centered around the investigation and mathematical modeling of the performance of High-Temperature Electrochemical Hydrogen Compression (HT-ECHC) cells. Despite the presence of various low-temperature ECHC mathematical models in existing literature, a notable gap exists in the lack of comprehensive studies focusing on cell-level and stack-level modeling for HT-ECHCs. The necessity for this study is further highlighted by the lack of HT-ECHC optimization studies and modeling efforts in the literature that are especially focused on pure hydrogen or reformate gas feeding. This thesis aims to add valuable information to the understanding and development of HT-ECHC systems while addressing these shortcomings.

1.3 Objective

The objectives of the thesis are as follows:

- To develop a cell-level HT-ECHC model for investigating the impacts of key parameters (e.g. cell temperature, reformate gas composition etc.) on the cell performance.
- To develop a cell-level HT-ECHC model that operates with both pure H_2 and reformate gas mixture.
- To validate the 0D modeling results (i-V characteristics) with the results of the experimental studies.
- Validation of the mathematical model established for both single cell and stack level ECHC cell with experimental results for the pressurization value obtained by considering the effect of back diffusion.

Within the scope of this thesis, HT-ECHC modeling was prepared in the MATLAB environment and the developed model was validated by comparing it with performance tests.

1.4 Thesis Outline

In the second chapter, hydrogen pressurization methods, literature research on ECHC, the general working principle and components of ECHC are introduced. Details on mathematical model techniques for ECHC design are provided.

In the third section, parameters and mathematical model approaches that determine the pressurization criteria for both single cell and stack model design of the ECHC cell are presented. The effect of back diffusion on cell performance was examined. Also, it is explained how to obtain polarization curves in the case of pure H_2 feeding and reformate gas feeding of the ECHC cell.

In the conclusion (Chapter Five), the results obtained from the analysis of the ECHC cell are presented.

CHAPTER TWO
BACKGROUND AND LITERATURE SURVEY

2.1 Hydrogen Compression Methods

According to the volume reduction principle, hydrogen is typically produced at low pressures (15–30 bars) and compressed for transportation (Durmus et al., 2021). In both industry and literature, gas phase hydrogen is compressed using both mechanical and non-mechanical compressors. Figure 1 provides a detailed explanation of the operating principles of mechanical and non-mechanical compressors.

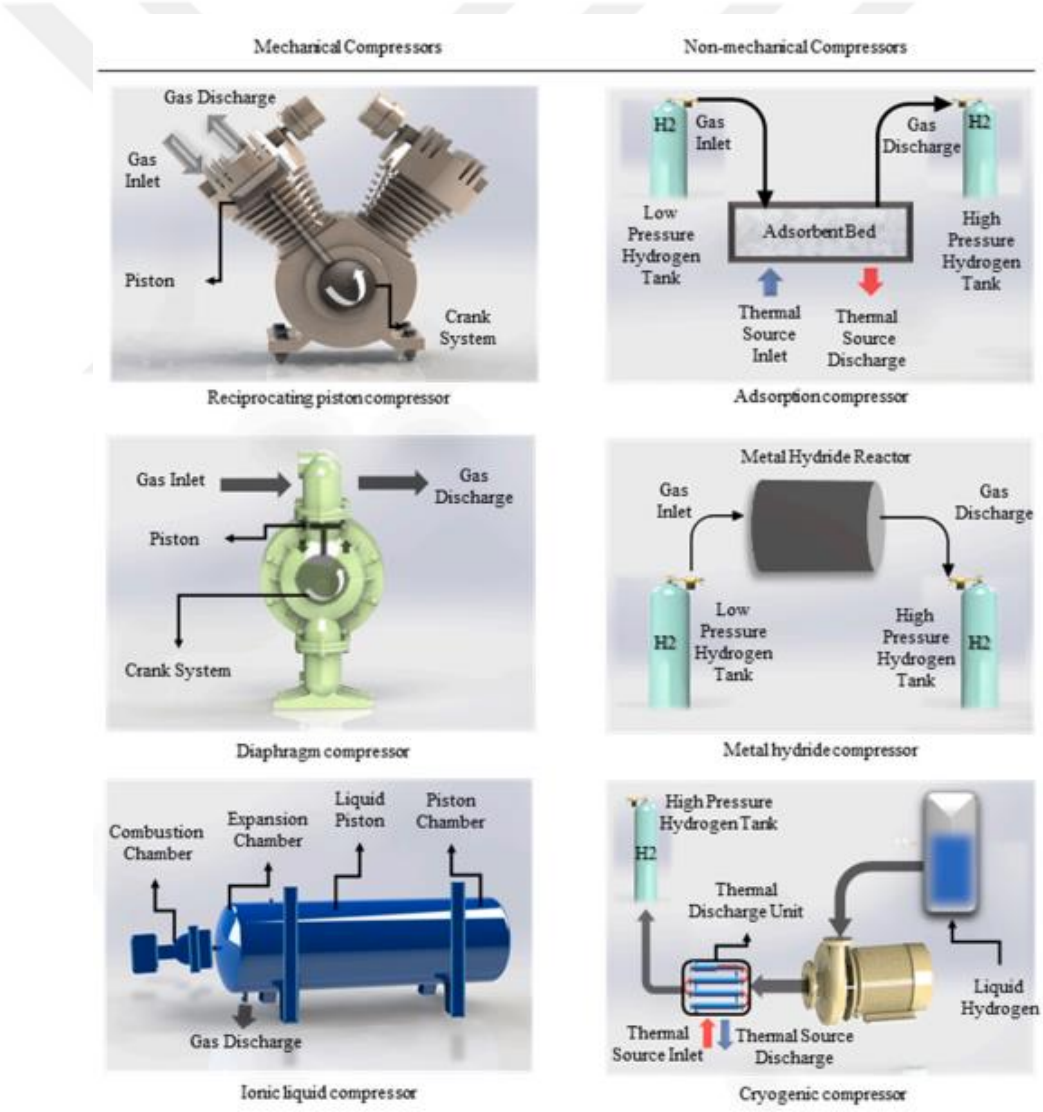

Figure 2. 1 Schematic representation of mechanical and non-mechanical hydrogen compressors (Durmus et al., 2021)

2.1.1 Mechanical Compressors

Mechanical compressors are usually preferred for compressing low-pressure hydrogen using mechanical energy, making them the most frequently used type of compressors. These compressors are employed to transfer hydrogen gas, by compressing it into smaller volumes, to high-pressure tanks. In this process, the closed volume of the gas decreases, leading to the attainment of higher gas pressures. In the literature, there are many studies on the compression ratios of mechanical compressors (Tahan, 2022). Outputs related to mechanical compressors can be examined in the relevant review articles of the literature. Contrary to the advantages of mechanical compressors, several disadvantages have been observed. Main reasons such as vibration, noise and high-power consumption have led researchers in this field to look for alternative pressurization methods.

2.1.1.1 Reciprocating Compressors

Reciprocating compressors are mechanical devices that work on the principle of converting rotational energy into reciprocating motion for the compression of gases, and consisting of basic components such as crankshaft, connecting rod, piston, and cylinder. An electric motor or internal combustion engine converts energy into rotational motion. This rotational energy is transferred to the crankshaft and converted into reciprocating motion with the help of the connecting rod, allowing the piston to move linearly in the cylinder. As the piston reciprocates within the cylinder, it undergoes a dynamic process that leads to the reduction of the gas volume and a simultaneous increase in pressure. This complex mechanism forms the basis of reciprocating compressors used in a variety of industrial applications, such as industrial air compression, air conditioning systems, oil and gas industry, and automotive applications. Comparing reciprocating compression to other compression techniques, a number may often conclude that it is outdated technology. Furthermore, problems like vibration-related difficulties, higher maintenance costs, higher production costs, and a reduction in heat transfer management system efficiency because of the reciprocating motion further complicate the choice of reciprocating

compressors. A reciprocating compressor stands out as a robust solution, effortlessly capable of achieving compression levels ranging between 70 MPa and 85 MPa (Zou et al., 2020) .

2.1.1.2 Diaphragm Compressors

The working principles of diaphragm compressors and reciprocating compressors are quite similar. Similar to reciprocating compressors, diaphragm compressors operate on the fundamental principle of positive displacement. A flexible diaphragm that enters and exits the compression chamber makes up the basic component of a diaphragm compressor. A vacuum is formed in the chamber when the diaphragm slides inward, enabling gas to enter. The gas then becomes pressured as the diaphragm expands and the pressure rises. As there is no direct contact between the fluid and the moving elements of the compressor, this type of compressor protects from contamination, oxidation, and fluid deterioration, making it perfect for applications needing high levels of purity (Sdanghi et al., 2019).

2.1.2 Non-mechanical Compressors

There are several options available to replace conventional mechanical hydrogen compressors; one prominent category consists of non-mechanical hydrogen compressors. The literature emphasizes a variety of kinds that are extensively used in various fields, such as cryo-compressors, adsorption compressors, metal hydride hydrogen compressors, and electrochemical hydrogen compressors. These cutting-edge technologies add to the variety of hydrogen compression techniques by providing clear benefits in terms of effectiveness, safety, and environmental impact Rhandi et al., (2020).

2.1.2.1 Absorption Compressors

The operation of absorption hydrogen compressors is dependent on the thermal interaction of the absorption bed. Thermal interactions fuel the pressured hydrogen gas

as it flows toward the high-pressure hydrogen tank after being transported from the low-pressure tank to the adsorbent body. For this kind of compressors, the thermal control principle is crucial. The compression range of the system is smaller than that of other systems since low-pressure hydrogen is used as an input (Sdanghi et al., 2020). Adsorption compressors are used as hydrogen compressors thanks to several basic advantages. Among their primary advantages, they can be given as examples of having a stable system, being safe due to low pressure operation, quiet operation and having no production-maintenance costs.

2.1.2.2 Metal Hydride Compressors

Bidirectional heat is used in metal hydride hydrogen compressors (MHCs) to interact between the metal and the hydride production. The major objective is to store hydrogen as well as compress it. The steps of the operating principle include absorption, chemical binding, compression, storage, and release. When hydrogen gas is to be used, heat energy acts as a motor, and an endothermic reaction causes the metal hydrides in the compressor to release hydrogen (Disli et al., 2023). Due to the hydrogen storage involved, this process is very interdisciplinary and useful. Moreover, compared to the gas and liquid phases, metal hydrides have a substantially higher storage density. One of the compressor's greatest drawbacks, in my opinion, is its size.

The advantages of MHCs systems include their ability to run on industrial waste heat, their high energy density, silent operation, and lack of moving components. The previously mentioned advantages demonstrate how readily MHCs can be included into hydrogen integrated systems.

However, MHCs waste energy during compression and have a lesser efficiency than conventional compressors. Examples of the mechanisms causing this energy loss are desorption processes and cooling activities.

2.1.2.3 Cryogenic Hydrogen Compressors

Cryogenic hydrogen compressors are the general name of compressor systems used to compress hydrogen gas at -252 ℃. In these devices, hydrogen is liquefied and compressed at high pressures. Basically, the supply of liquid hydrogen is a key case for the operation of the system. The system additionally includes a heat exchanger. Here, hydrogen gas undergoes a heat exchanger before converting from liquid phase to gas form. The main purpose is to increase the gas temperature and provide a suitable temperature environment in the next compression process. Mechanical compressor methods can also be used for compression. The most frequently used cryogenic tank-diaphragm type compressors in the literature. Like metal hydride hydrogen compressors, this method can also be conveniently used for hydrogen gas distribution or storage in cryogenic hydrogen compressors (Sadaghiani & Mehrpooya, 2017).

2.2 Electrochemical Hydrogen Compressors

Green energy resources and technologies are crucial since the number of available fossil fuels will be insufficient to satisfy the expanding global population's energy needs in the coming years. Many studies on green hydrogen production systems have been published in the literature (Dincer & Acar, 2018). The produced hydrogen needs to be compressed if hydrogen is to be stored in a pressurized tank. In this regard, the electrochemical hydrogen compressor (ECHC) emerges as a technology that can be used both in hydrogen refueling systems for vehicles and for pressurizing hydrogen in containers (Chouhan, Bahar, et al., 2020). In addition to pressurization, the fact that it can purify hydrogen in the situation of reformate gas feeding makes this technology more advantageous. It basically consists of 3 main parts: anode plate, cathode plate and membrane that provides gas flow. Each part of the ECHC cell has its own importance, but membranes have a special importance because they are the most important part that drives the gas flow and the passage of ions. There are two different ECHC groups operating at two different operating temperatures: high temperature (greater than 100°C) and low temperature (below 100°C). In high temperature ECHCs, the membrane must be thermally and structurally resistant in order not to lose

its mechanical integrity. PBI membrane is known to be used in high-temperature fuel cells due to the high mechanical and thermal resistance it provides (Chandan et al., 2013), therefore the use of PBI membrane in the electrochemical hydrogen compressor also has the benefits of the aforementioned advantages.

The components of the ECHC cell are explained in the most basic way as follows. It is a device made up of a Membrane Electrode Assembly (MEA) that is placed between two bipolar plates which has flow channels for hydrogen flow. A 3-D representation of the components of the ECHC cell is shown in Figure 2.2. The description and functions of other components included in the ECHC are explained in detail in the following section.

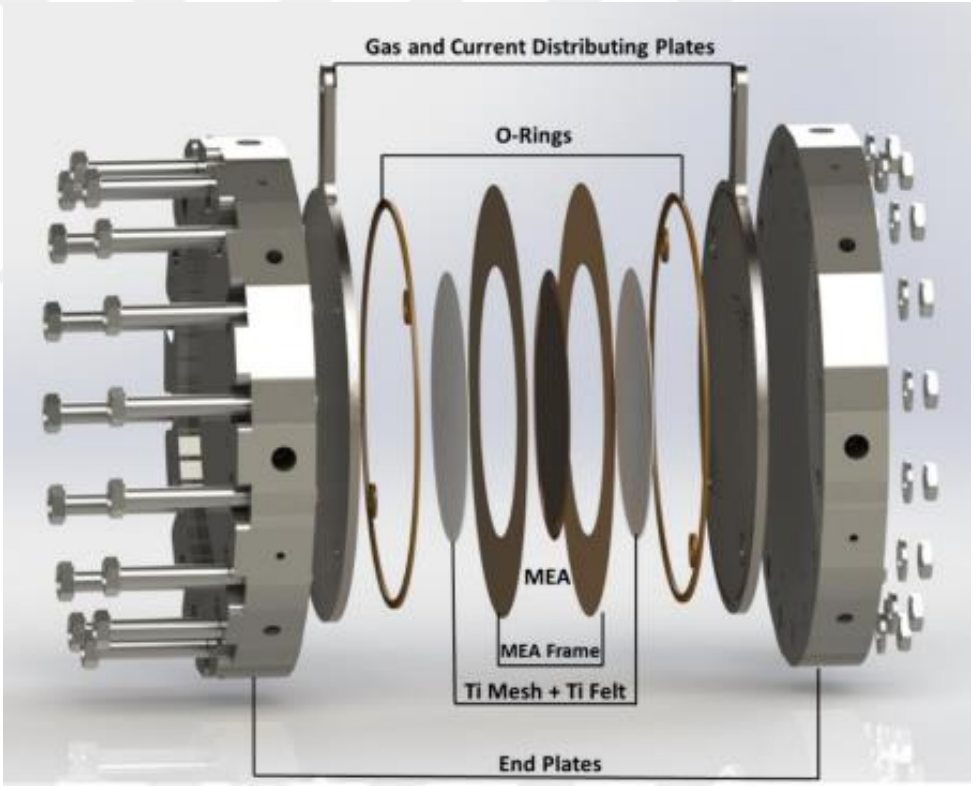

Figure 2. 2 ECHC components, Bulanık Durmuş et al., (2024)

2.2.1 Membranes

Membranes are located in the middle of the ECHC cell and are one of the elements that most affect cell performance by ensuring the transfer of hydrogen ions formed as

a result of the oxidation reaction occurring at the anode to cathode. Considering the high-pressure levels that exist inside the cell, it is crucial to select a membrane with the ideal thickness to prevent any punctures or abrasions in the membrane. To ensure ion transfer, which is the most important function of the membrane, a membrane with high ion conductivity and thermal resistance should be chosen. In ECHC cells, operating temperatures above 100°C are considered high temperature values, while operating temperatures below this value are called low temperature values. While Perfluorosulfonic (PFSA) or Nafion membranes are generally preferred in ECHC cells operating at low temperatures, Polybenzimidazole (PBI) membranes are generally preferred for ECHC cells operating under high temperature conditions due to their thermal resistance values (Mench, 2008).

2.2.2 Catalyst

The catalyst layer plays an important role in accelerating electrochemical reactions and facilitating the pressurization process. The catalyst acts as a place for hydrogen gas to separate protons and electrons. As the reaction rate increases, a more efficient pressurization process occurs. The use of the catalyst layer is inevitable in experimental setups and industrial applications where high pressures are required. In light of the studies reported in the literature, the most used catalyst is the Pt-based catalyst layer due to its efficiency and fast reaction Mench, (2008).

2.2.3 Gas Diffusion Layer

A porous gas diffusion layer (GDL) increases reactant gases diffusion to active catalyst areas via flow channels Mench, (2008). These layers may have microporous or macroporous structures. The thermophysical properties of these materials are very important for the continuity and efficiency of the reaction. In addition to high electrical conduction coefficient, mechanical strength and appropriate porosity values, it must provide chemical stability under high pressure Marciuš et al., (2022).

2.2.4 Bipolar plates and end plates

Bipolar plates are another important component of the ECHC cell. These plates allow the gas to flow homogeneously with the flow channels they have. In addition to containing flow channels, providing good mechanical strength and good electrical conduction are among the must-have features. Since flow channels will directly affect cell performance, the production method and material technology of bipolar plates are very important. Bipolar plates produced with a material that is not resistant to corrosion will corrode and rust in long-term use. This will have a negative impact on cell efficiency and cause a decrease in performance. Within the scope of all the mentioned features, the most commonly used endplate material in the literature is stainless steel derivatives. Leng et Al., (2020) performed the weight reduction study by determining the optimum geometric properties of the endplate. As a result, uniform pressure distribution and weight optimization were determined. They also mentioned production methods in their studies Leng et Al., (2020). Figure 2.3 represents the schematic representation of plastic forming methods of bipolar plates.

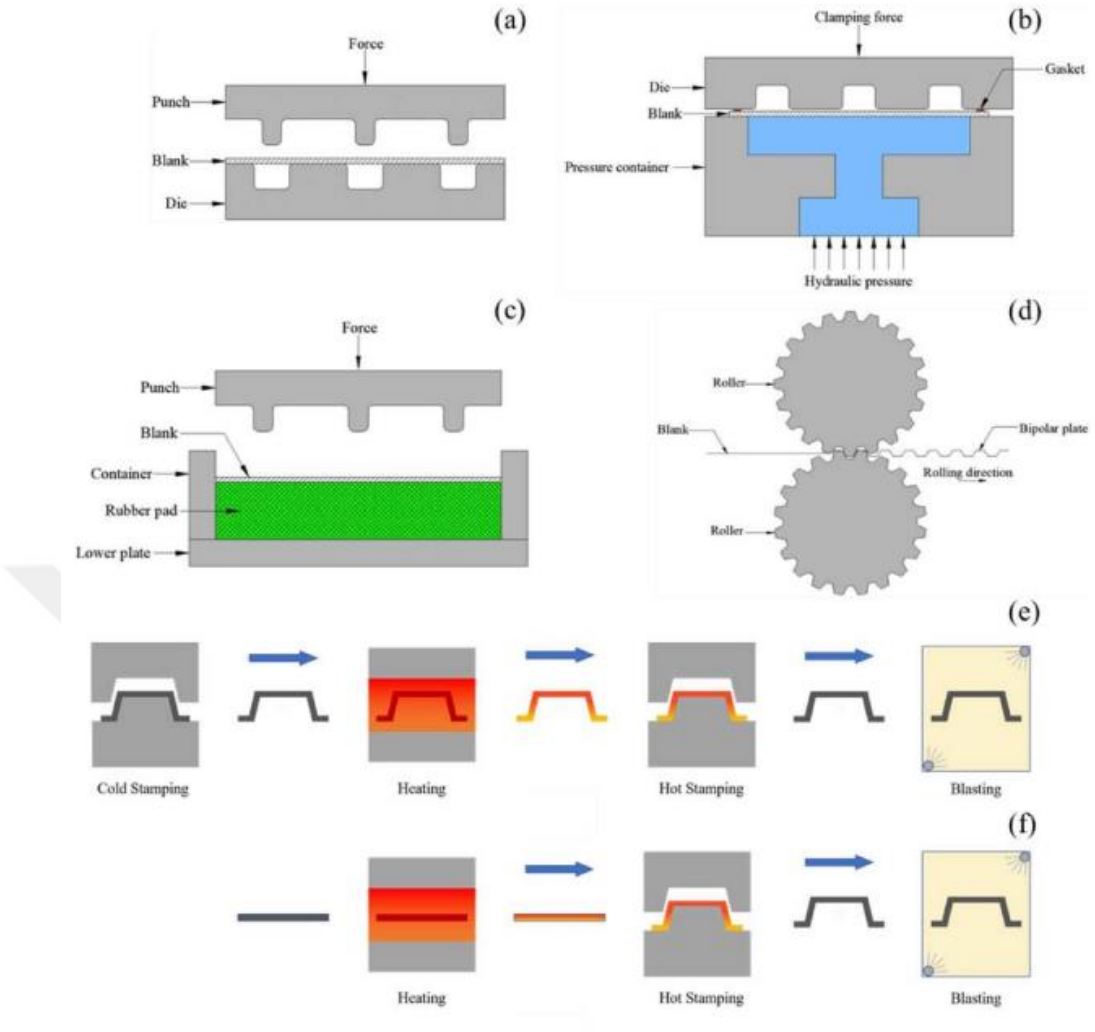

Figure 2. 3 Diagram showing the plastic forming techniques used to create BPPs made of stainless steel (a)stamping (b) hydroforming (c) rubber pad forming (d) direct roll forming Leng et al., (2020)

End plates are, as their name implies, the components that are mounted to the outermost ECHC cells. Their most basic function is to protect the integrity of other cell elements and keep them together under high pressure. At the same time, they must have very good thermal resistance and prevent possible gas leaks.

2.3 Literature Survey

In this section, the studies on the electrochemical hydrogen compressors are examined and the results obtained by the researchers are presented. Mathematical modeling is a technique used to examine the systems' performance under different working conditions. Considering the scarcity of research on mathematical modeling of ECHC in existing literature, it is quite challenging to determine the relevant parameters for ECHC, but there are still a few studies done on this topic. For example, (Bampaou et al., 2018) investigated a zero-dimensional mathematical model for an ECHC that can operate up to 343 K and 150 bar, indicating that the back diffusion phenomenon is mostly accountable for losses at low current densities. (Nordio et al., 2019) assessed the performance of an ECHC using a 1D + 1D model and solved the system of equations using MATLAB. They demonstrated that as temperature rises, membrane conductivity increases, resulting in a reduction of ohmic resistance. (Toghyani et al., 2020) performed a 3D computational fluid dynamics (CFD) model for an EHC to study its thermal and electrochemical characteristics. They showed that an increase in the pressure and the thickness of gas decreases the cell performance. In another study of the same group, used exergy analysis together with a CFD model of ECHC to observe the exergy-based cost of H_2. They found that decreasing GDL thickness also decreases the exergy-based cost. With a highly efficient PEM-based electrochemical hydrogen compressor, compressing to 54 bar is conceivable, and with an upgraded sealing structure and cell design, this value can be increased to above 100 bar Ströbel et al.. (2002). (Chouhan, Bahar, et al., 2020) showed that with a Nafion 115 membrane type based ECHC operating at room temperature, the values exceeding 150 bar may be obtained at a low operating voltage of 0.1 V. Back diffusion, which is one of the most critical factors determining ECHC performance, was also highlighted in their study, and its impact on performance was investigated. Because working at lower voltages reduces the relevant compression ratio, the value of back diffusion decreases, resulting in better ECHC efficiency. Rohland et al., (1998) achieved compression up to 43 bar in a low-temperature ECHC having Nafion 117 as the membrane. A study employing 0-D modeling through Mathematica software was conducted to determine the energy demand for electrochemical compression across various outlet pressure scenarios. The

energy required for compression was found to increase with pressure Dale et al., (2007).

Studies on the mathematical modeling of ECHC found in the literature is presented in Table 2.1.

Table 2. 1 Studies on the mathematical modeling of ECHC found in the literature

References	Membrane Type	Method	Findings of the Study
Toghyani et al. (2020)	-	• The study employs a 3D numerical method with the single-domain approach to simulate both thermal and electrochemical behaviors within the electrochemical cell.	• The cell performs better and requires less voltage at higher working temperatures. • At smaller GDL thicknesses, less total voltage is needed. • The performance of the EHC is little impacted by the porosity of GDL. • When the channel width changes between 1 to 2 mm, the electrochemical compressor's needed voltage has improved by 40%.
Toghyani et al. (2020)	Nafion	• A 3D numerical model was created using ANSYS Fluent for ECHC. • Single cell outcomes are expanded to include the whole ECHC stack.	• A temperature increase of 363 K to 393 K causes a 2.5% change in cell voltage. • Using 50% less GDL thickness results in a 53% reduction in the exergy cost of hydrogen. • By raising the cathode pressure from 1 bar to 20 bars, the energy and exergy efficiency of the EHC stack declines from 55% to 44% and from 92% to 82%, respectively. • As the operating temperature increases from 363 K to 393 K, resulting in a 0.5% decrease in hydrogen exergy cost, the energy and exergy efficiency of the ECHC stack show an enhancement of approximately 3.1%.

Table 2. 1 continued.			
Dale et al. (2007)	Nafion	• Using Mathematica software, 0D modeling was performed to determine the energy needed for electrochemical compression at various output pressures.	• The activation and ohmic polarizations are the main drivers of cell voltage. • As pressure rises, more energy is needed for compression.
Sdanghi et al. (2019)	Nafion	• In addition to doing experimental research, a pseudo-2D model was created.	• Using thick membranes resulted in an uneven water transfer across the membrane. The membrane experienced localized dehydration due to high humidity levels.
Bampaou et al. (2018)	Nafion	• An AspenPlus-based 0D ECHC model (temperature: up to 343 K; pressure: up to 15 MPa) was constructed to compute overall voltage, factoring in Nernst voltage, ohmic loss, and activation overpotential.	• Higher cooling loads are the outcome of higher humidifier temperatures. • The primary voltage loss is ohmic overvoltage; greater current densities make the activation loss visible. • The primary efficiency decline stems from hydrogen back diffusion.
Nordio et al. (2019)	Nafion	• A 1D + 1D Matlab model has been used to simulate the EHC performance. • A number of input factors have been studied, including the cathode pressure, hydrogen inflow concentration, total inlet flow rate, and feed contamination.	• Following a pure H_2 feed, three distinct mixtures—H_2-CH_4, H_2-He, and H_2-N_2—have been tested. When the H_2 concentration is at its greatest with He feed, the purest value is attained.
Chouhan et al. (2020)	Nafion	• The method involves testing the electrochemical hydrogen compressor equipped with a Nafion membrane using a single-cell setup featuring a 25 cm2 active surface area.	• The electrochemical hydrogen compressor's performance is significantly impacted by back-diffusion.

Table 2. 1 continued.			
Chouhan et al. (2020)	Nafion	• The outputs of series and parallel-connected ECHC cells have been examined and compared.	• While the ESFS design can give greater pressures but lower flow rates, the ESFP configuration can deliver higher gas throughput but only at restricted pressures.

CHAPTER THREE
MATHEMATICAL MODEL

3.1 Working Principle of ECHC

Electrochemical hydrogen compressors (ECHCs) are devices that can be used to pressurize hydrogen and purify it if a gas mixture containing H_2 is fed. As can be seen in Figure 3.1, pure hydrogen or H_2 found in the reformate gas entering the compressor is separated into electrons and protons (H_2 oxidation reaction, Equation (3.1)). The membrane in the middle acts as a filter and allows only protons to pass. In addition, electrons pass to the cathode side through an external circuit, and protons recombine with these electrons and turn into H_2 molecule (H_2 evolution reaction, Equation (3.2)). This process continues as long as feed gas is supplied and with time, the H_2 amount in the cathode region and the pressure at the cathode side increase.

$$H_2(P_A) \rightarrow 2H^+ + 2e^- \tag{3.1}$$

$$2H^+ + 2e^- \rightarrow H_2(P_c) \tag{3.2}$$

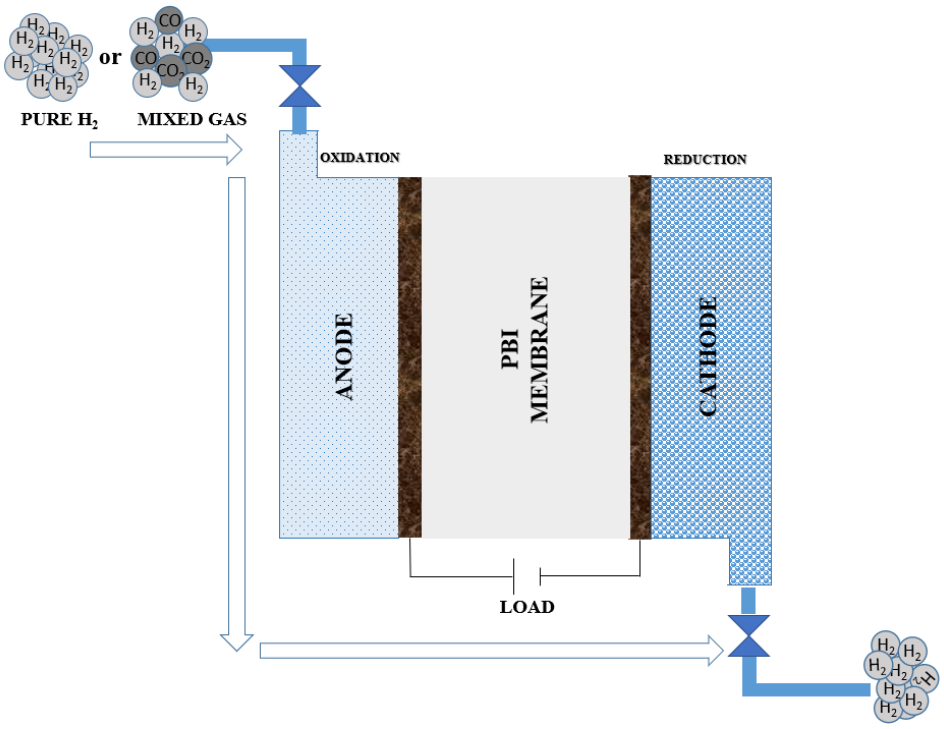

Figure 3. 1 Schematic view of ECHC working principle

3.1.1 High-Temperature ECHC Semi-Experimental Mathematical Model Development

The Nernst equation is an expression of an established thermodynamic equilibrium and is an expression for the open circuit voltage dependent on temperature and pressure. The general equation for Nernst voltage is written as shown in Equation (3.3) (Mench, 2008).

$$E_{\text{Nernst}} = \frac{\text{RT}}{2\text{F}} \ln\left(\frac{P_{\text{Cathode}}}{P_{\text{Anode}}}\right) \tag{3.3}$$

Where P_{Cathode} is the cathode's absolute pressure, P_{Anode} is the anode's absolute pressure, T is the operating temperature (K).

If $\alpha_{anode} = \alpha_{cathode}$ the activation overpotential at the anode and cathode part is calculated from Equation (3.4) and (3.5), respectively (Mench, 2008).

$$E_{Activation,a} = \frac{R \cdot T}{\alpha_{anode} \cdot F} sinh^{-1}\left(\frac{i}{2 \cdot i_{o,anode}}\right) \tag{3.4}$$

$$E_{Activation,c} = \frac{R \cdot T}{\alpha_{cathode} \cdot F} sinh^{-1}\left(\frac{i}{2 \cdot i_{o,cathode}}\right) \tag{3.5}$$

Where, i is the current density (A/cm^2), $i_{o,anode}$ is the anodic exchange current density (A/cm^2), $i_{o,cathode}$ is the cathodic exchange current density (A/cm^2), α is the charge transfer coefficient.

The ohmic voltage can be represented as Equation (3.6) (Nalbant et al., 2018):

$$E_{ohmic} = i\left[\left(\frac{t_{ACL}/2}{\sigma \cdot \varepsilon_a} + \frac{t_M}{\sigma} + \frac{t_{CCL}/2}{\sigma \cdot \varepsilon_c}\right) + \left(\frac{A_{cell} \cdot R_{contact}}{A_{contact}}\right)\right] \tag{3.6}$$

where t_M is the membrane thickness (cm), and σ is the ionic conductivity of the membrane (S/cm), t_{ACL} and t_{CCL} are the thicknesses of anode and cathode catalyst

layers (cm), ε_a and ε_c porous coefficient of anode and cathode side respectively, $A_{contact}$ is the contact area (cm^2), and $R_{contact}$ is the contact resistance ($\Omega \cdot cm^2$).

The total cell voltage can be determined by adding the Nernst voltage, the anode and cathode overvoltage, and the ohmic voltage. The cell voltage equation can be written as Equation (3.7). Concentration losses are included in the Nernst and activation overvoltage. Other losses due to electric short circuit, the species crossover through the membrane, electron leakage, or contamination of the components are neglected.

$$E_{Cell} = E_{\text{Nernst}} + E_{Activation,a} + E_{Activation,c} + E_{ohmic} \tag{3.7}$$

The values of the main parameters used in the model are presented in Table 3.1.

Table 3. 1 Parameters used in the analysis of the semi-empirical model (Durmuş, 2023)

Symbol	Value	Unit	Definition
T	413-453	K	Operation Temperature
P_a	101325	Pa	Anode Pressure
σ	8.3	S/m	Membrane Conductivity
t_m	$6 \cdot 10^{-5}$	m	Membrane Thickness
A_{cell}	0.002304	m^2	Aktive Area
α_a	0.5	-	Anodic Exchange Current Density
α_c	0.5	-	Cathodic Exchange Current Density
t_{ACL}	10^{-8}	m	Thickness of Anode Catalyst Layer
t_{CCL}	10^{-8}	m	Thickness of Cathode Catalyst Layer
$A_{contact}$	0.0006912	m^2	Contact Area
ε_a	0.5	-	Anode Porosity Coefficient
ε_c	0.5	-	Cathode Porosity Coefficient

3.1.2 Investigating Back Diffusion's Effect on a Single Cell ECHC Performance Using Mathematical Modeling

In this section, it is aimed to observe the net H_2 flow rate by examining the forward and backward flow rate of a single-cell HT-ECHC change with time at a constant temperature, under different cell voltage values, and to determine the pressure value that the HT-ECHC cell will reach with the ideal gas approach and validate it with experimental data.

The following assumptions are used in the modeling.

- Ideal gas law is considered to be valid for the calculation of cathode pressure.
- Initially, the anode and cathode parts are at atmospheric pressure.
- Hydrogen that was 99.999% pure was used to feed a 100 cm^2 cell.
- Losses in cables are disregarded, and fixed cell voltages of 0.1 V, 0.2 V, 0.4 V, 0.6 V, 0.8 V, 1 V, and 1.5 V remain constant during the experiment.

All equations specified from Equation (3.8) to Equation (3.16) (given in Section 3.1.2.1) were integrated into the MATLAB program by making the previously mentioned assumptions. The cell voltage was maintained constant at certain values, and investigations were performed separately for each voltage value. At these cell voltages, the current values drawn by the ECHC cell from the power source were noted and a curve showing the current change over time was created. The curve showing the current change of the cell with time is the most important input needed to validate the model. As it will be recalled, the anode and cathode sides were assumed to be at atmospheric pressure, and the hydrogen pressure accumulated at the cathode was calculated at each time step after the initiation of the operation. The net hydrogen molar flow rate is one of the most crucial variables required to determine the pressure using the ideal gas law. To obtain this parameter, firstly, the forward molar flow rate was calculated with Faraday's law using the data showing the current change over time during the experiment, and the net molar flow rate was obtained by calculating the backward hydrogen molar flow rate caused by back diffusion due to the pressure

difference between the cathode and the anode. In the final case, by obtaining Equation (3.12), a model that gives the pressure formed at the cathode using the variation of the current with time is created. The model was validated using this approach.

In examining the effect of back diffusion on ECHC performance, the results of the study by Chouhan, Bahar, et al., (2020) was first used for validation. The effect of back diffusion on ECHC was examined with reference to the study of using Nafion 115 membrane at room temperature. In the current context (section 3.1.2.1), the stages of creating a comprehensive mathematical model on the Electrochemical Hydrogen Compressor (ECHC) are presented, focusing on its performance and functionality, considering the effect of back diffusion, especially in the context of single-cell design configuration.

3.1.2.1 Mathematical Equations and Modeling Approach for Single Cell ECHC

The forward and backward H_2 molar flow rates were initially computed using the change of cell current with time Equation (3.8). The forward molar flow rate, which expresses the amount of H_2 flowing from the anode to the cathode can be determined using Faraday's law (Chouhan, Bahar, et al., 2020).

$$\dot{n}_f = \frac{I(t)}{n \cdot F} \tag{3.8}$$

During the operation of HT-ECHCs, the protons passing through the membrane are reduced at the cathode side, increasing the amount of H_2 accumulated. This increase also increases the pressure of the cathode part. Since the anode side is kept constant at atmospheric pressure, a pressure difference will occur between the anode and cathode parts. Therefore, due to the pressure difference, an undesirable backward flow from the cathode to the anode occurs, causing a phenomenon called back diffusion, which negatively affects the performance of the cell. The backward flow rate is calculated using Equation (3.9), which combines Henry's and Fick's laws. As seen in this equation, back diffusion is inversely proportional to the membrane thickness while

being directly proportional to the cell active area, the pressure difference between the cathode and anode, and the permeability coefficient of the membrane. Since the anode side remains constant under atmospheric pressure, it can be expected that the backward flow rate will rise when high-pressure values are obtained (Chouhan, Bahar, et al., 2020).

$$\dot{n}_b = \frac{D_H \cdot A \cdot (P_c(t) - P_a)}{d} \tag{3.9}$$

The net H_2 molar flow rate was obtained by subtracting the backward flow rate from the forward flow rate. The expression used to calculate the amount of net H_2 flow rate is shown in Equation (3.10).

$$\dot{n}_n = \dot{n}_f - \dot{n}_b = \frac{I(t)}{2 \cdot F} - \frac{D_H \cdot A \cdot (P_c(t) - P_a)}{d} \tag{3.10}$$

Equation (3.11) can be used to express the net molar flow (mol/s) of H_2 under the assumption that H_2 acts like an ideal gas.

$$\dot{n}_n = \dot{n}_f - \dot{n}_b = \frac{\dot{P}_c V_c}{RT} \tag{3.11}$$

Where $\dot{P}_c$ represents the cathode pressure increase rate (Pa/s), V_c represents the cathode volume (m^3).

By combining Equations (3.10) and (3.11), the cathode pressure change over time can be calculated from Equation (3.12).

$$\frac{\dot{P}_c V_c}{RT} = \frac{I(t)}{2 \cdot F} - \frac{D_H \cdot A \cdot (P_c(t) - P_a)}{d} \tag{3.12}$$

3.1.2.2 Performance Evaluation Parameter (Single Cell)

It is possible to express the work performed by an ideal compressor, which is expected to operate under isothermal conditions, by using Equation (3.13) (Chouhan, Bahar, et al., 2020).

$$W_{ideal}(t) = n_n(t)RTln\left(\frac{P_c(t)}{P_a}\right) \tag{3.13}$$

As can be seen in Equation (3.14), the product of the applied cell voltage (E_{cell}) and the total charge transferred (Q(t)) yields the actual work done by the HT-ECHC cell (Chouhan, Bahar, et al., 2020).

$$W_{actual}(t) = E_{cell}Q(t) = E_{cell}\left(2Fn_f(t)\right) \tag{3.14}$$

ECHC efficiency can be found by dividing the compressor's ideal work by its actual work. Thus, the efficiency of the HT-ECHC cell can be determined by proportioning the Equations (3.13) and (3.14) shown above.

$$\eta_{cell}(t) = \frac{W_{ideal}(t)}{W_{actual}(t)} = \frac{n_n(t)RTln\left(\frac{P_c(t)}{P_a}\right)}{E_{cell}(2Fn_f(t))} = \left[\frac{\frac{RT}{2F}ln\left(\frac{P_c(t)}{P_a}\right)}{E_{cell}}\right]\left[\frac{n_f(t) - n_b(t)}{n_f(t)}\right] \tag{3.15}$$

The primary term on the right side in Equation (3.15) indicates the voltage efficiency and the second term gives the current efficiency. Thus, Equation (3.15) can also be shown in Equation (3.16).

$$\eta_{cell}(t) = \eta_{Voltage}(t)\eta_{Current}(t) \tag{3.16}$$

3.1.3 Investigating Back Diffusion's Effect on a Stack Level ECHC Performance Using Mathematical Modeling

In examining the effect of back diffusion on ECHC performance, (Chouhan, Aryal, et al., 2020) was taken as reference while conducting this study. In this context, ECHC was examined in stack-level.

3.1.3.1 Mathematical Equations and Modeling Approach for Stack Level ECHC

The single-cell electrochemical hydrogen compressor's mathematical modeling was thoroughly detailed in the section of 3.1.2.1, and the pressure value obtained was shown under the title of results validated with experimental values. This section discusses the mathematical modeling strategy for an electrochemical hydrogen compressor stack model consisting of five series-connected cells. A typical electrochemical hydrogen compressor with series connections is defined as a system where the feed gas and electrical load are both linked in series. The gas injected into the anode in the single-cell ECHC model was split into protons, converted into hydrogen molecules with an external charge, and compressed on the cathode side to achieve a specific pressure value. The most important point to consider in series connected stack ECHC design is that the cathode pressure of each cell in between is equal to the anode pressure of the other cell. In other words, the outlet pressure of the intermediate cells is equal to the inlet pressure of the adjacent cell. In the series-connected stack ECHC model, the cell voltage is distributed equally to each cell, and the current is constant for each cell. These will be explained in more detail when forward and backward flow calculations are made. A detailed schematic illustration of the stacked model can be found in Figure 3.2. The amount of pressure increases from left to right (Chouhan, Aryal, et al., 2020).

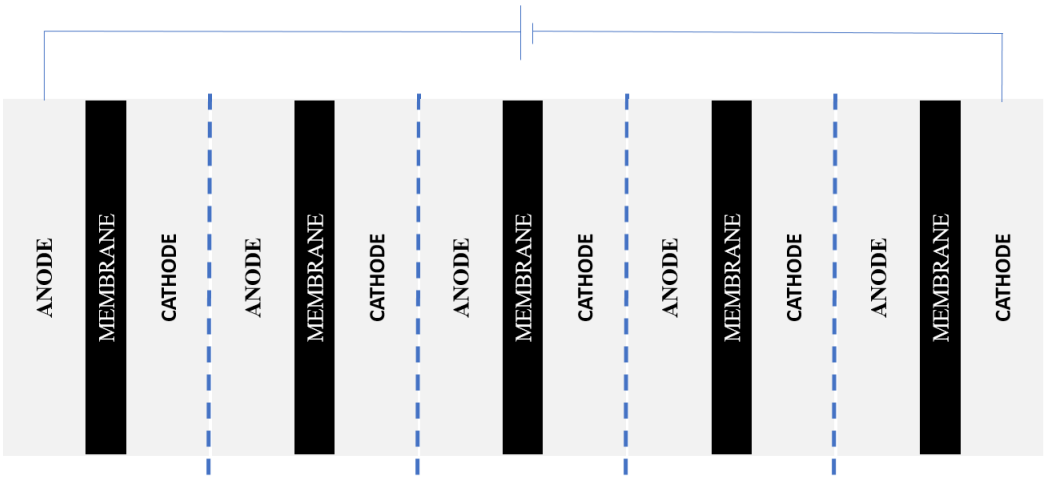

Figure 3. 2 Schematic representation of the series-connected stack ECHC model

To perform a reliable analysis, equations for each volume must be created separately by dividing each cell by the control volume. Figure 3.3 represents the control volume (CV) of the 5-cell stacked ECHC design. The first control volume (CV:1) consists of the anode part of the first cell. Since it is a series-connected system, the forward molar flow rate expressed by green arrows has the same value for each cell, since the current is of equal value for each cell. The backward molar flow rate due to the pressure difference between the cathode and anode, represented by red arrows, is shown for each control volume. The last control volume contains the cathode part of the last cell. Thus, a control volume (N+1) more than the number of cells (N) is formed.

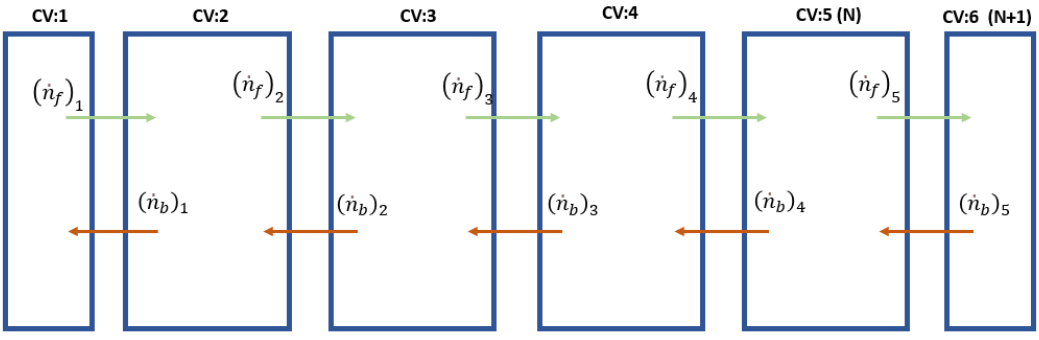

Figure 3. 3 Schematic layout of the control volumes of the series connected stack ECHC model

At this stage, the formulas used in mathematical modeling and the modeling approach are explained. First, to calculate the net hydrogen molar flow rate, the

incoming and outgoing hydrogen molar flow rate must be written for each control volume. To calculate the net molar flow rate, the balance is established as in Equation (3.17).

$$\sum \dot{n}_{net,in} - \sum \dot{n}_{net,out} = \frac{\dot{P}_{CV} \cdot V_{CV}}{R \cdot T} \tag{3.17}$$

The equilibrium for control volume 2 is shown in Equation (3.18).

$$\left[\left(\dot{n}_f\right)_1 - (\dot{n}_b)_1\right] - \left[\left(\dot{n}_f\right)_2 - (\dot{n}_b)_2\right] = \frac{\dot{P}_2 \cdot V_2}{R \cdot T} \tag{3.18}$$

The forward and backward hydrogen molar flow rate equations were previously expressed in Equations (3.8) and (3.9), if these equations are substituted in Equation (3.19):

$$\left[\frac{I(t)}{2 \cdot F} - \frac{D_H \cdot A \cdot (P_2(t) - P_1)}{d}\right] - \left[\frac{I(t)}{2 \cdot F} - \frac{D_H \cdot A \cdot \left(P_3(t) - P_2(t)\right)}{d}\right] = \frac{\dot{P}_2 \cdot V_2}{R \cdot T} \tag{3.19}$$

It was mentioned that in series connected systems, since the current is constant for each cell, the forward molar flow rate is also constant. In this case, the forward molar flow ratees will cancel each other in Equation (3.19). Therefore, the new expression will be as shown in Equation (3.20).

$$\left[\frac{D_H \cdot A \cdot \left(P_3(t) - P_2(t)\right)}{d}\right] - \left[\frac{D_H \cdot A \cdot (P_2(t) - P_1)}{d}\right] = \frac{\dot{P}_2 \cdot V_2}{R \cdot T} \tag{3.20}$$

When it is simplified Equation (3.20), the expression becomes as in Equation (3.21).

$$\frac{D_H \cdot A}{d}(P_3 - 2P_2 + P_1) = \frac{\dot{P}_2 \cdot V_2}{R \cdot T} \tag{3.21}$$

If the constant parameters are consolidated under a coefficient denoted as "k," this aggregation serves the purpose of simplifying the equations, providing a more simple and streamlined representation,

$$k = \frac{V_2 \cdot d}{DH \cdot A \cdot R \cdot T} \tag{3.22}$$

In this case, the final form of the equation is;

$$(P_3 - 2P_2 + P_1) = \dot{P}_2 \cdot k \tag{3.23}$$

When these operations are performed on each control volume, the same equations are obtained up to the control volume number N. Thus, the equations to be obtained up to volume N = 5 can be expressed in equations (3.23), (3.24), (3.25).

$$(P_4 - 2P_3 + P_2) = \dot{P}_3 \cdot k \tag{3.24}$$

$$(P_5 - 2P_4 + P_3) = \dot{P}_4 \cdot k \tag{3.25}$$

$$(P_6 - 2P_5 + P_4) = \dot{P}_5 \cdot k \tag{3.26}$$

Equation (3.27) can be used to calculate the amount of pressure in the last numbered control volume.

$$\left[\frac{I(t)}{2 \cdot F} - \frac{D_H \cdot A \cdot (P_6(t) - P_5(t))}{d}\right] = \frac{\dot{P}_6 \cdot V_6}{R \cdot T} \tag{3.27}$$

After the equations explained in detail above are analyzed and their explicit forms are obtained, the resulting matrix is as shown below. The created matrix was solved in the Matlab environment and the pressurization values in each cell were obtained and finally the outlet pressure was found.

$$\begin{bmatrix} -2\Delta t - k & \Delta t & 0 & 0 & 0 \\ \Delta t & -2\Delta t - k & \Delta t & 0 & 0 \\ 0 & \Delta t & -2\Delta t - k & \Delta t & 0 \\ 0 & 0 & \Delta t & -2\Delta t - k & \Delta t \\ 0 & 0 & 0 & 1 & -1 - k \end{bmatrix} * \begin{bmatrix} P_2(t) \\ P_3(t) \\ P_4(t) \\ P_5(t) \\ P_6(t) \end{bmatrix} = \begin{bmatrix} (-P_2(t-1) \cdot k - P_1 \Delta t \\ -P_3(t-1) \cdot k \\ -P_4(t-1) \cdot k \\ -P_5(t-1) \cdot k \\ \left(-P_6(t-1) \cdot \frac{k}{\Delta t}\right) - \left(\frac{I(t)}{2F} * \frac{d}{DH \cdot A}\right. \end{bmatrix}$$

3.2 Calibration of the Modeling Parameters using PSO Algorithm

Electrochemical hydrogen compressors consist of 3 basic parts as anode, cathode, and membrane. It is a device that can make purification thanks to the membrane in the middle while compacting with the principle of reducing the hydrogen at the cathode by taking electrons from an external charge source after oxidation at the anode. The major issue with modeling is that there is not much research on this topic in the literature, thus there is not much data regarding the variables, which have a big impact on reaction kinetics. The anodic and cathodic exchange current density is one of these parameters. Therefore, due to the similarity of reaction kinetics, it can be used as an alternative to calculate these parameters from some high-temperature fuel cell studies and electrolyzer studies. (Cheddie & Munroe, 2006) provide a one-dimensional mathematical model that forecasts how well a PEMFC using a PBI membrane will perform in terms of polarization and investigate the conductivity of the PBI membrane.

In this section, mathematical modeling of the experimentally obtained current-voltage curve of the electrochemical hydrogen compressor at a certain temperature was carried out, and the parameters needed for the modeling were calculated with the Particle Swarm Optimization method in Matlab, and obtained results were validated using experimental data.

A PBI membrane-based electrochemical hydrogen compressor cell with 100 cm^2 active area at 160°C was used in the experiment. With a pure H_2 supply, the current the cell uses from the used power supply whose voltage is kept constant is noted. This process was continued until the current value drawn from the power source reached equilibrium. Equations (3.25) and (3.26) for the anode and cathode sides, respectively, represent how to calculate the activation overpotential value corresponding to a certain energy value for the electrode reactions to occur Kulikovsky, A. A. (2019).

$$E_{Activation,a} = \frac{RT}{2\alpha_{anode}F}\ln\left(\frac{i}{i_{o,anode}}\right) \quad (3.25)$$

$$E_{Activation,c} = \frac{RT}{2\alpha_{cathode}F}\ln\left(\frac{i}{i_{o,cathode}}\right) \quad (3.26)$$

Where, i represents the current density (A/cm^2), $i_{o,anode}$ represents the anodic exchange current density (A/cm^2), $i_{o,cathode}$ represents the cathodic exchange current density (A/cm^2), α_{anode} and $\alpha_{cathode}$ represent the anode and cathode exchange transfer coefficient, respectively.

The lack of ECHC studies in the literature and the lack of sharing of some kinetic parameters is one of the most important problems encountered in mathematical modeling. It is especially difficult to calculate the value of exchange current density parameters that affect reaction kinetics. The Tafel Equation (3.27) shown below is used to calculate the exchange current density value Cao, (2017).

$$i_{0a,c} = i_{0a,c}^{ref} exp\left(-\frac{E_A}{R}\left(\frac{1}{T} - \frac{1}{T_{ref}}\right)\right) \quad (3.27)$$

The change of membrane proton conductivity depending on temperature is calculated by using the Arrhenius Equation (3.28) Özdemir et al., (2017).

$$\ln(\sigma T) = \ln(\sigma_0) - \frac{E_a}{RT} \quad (3.28)$$

Particle Swarm Optimization (PSO) was introduced in 1995 by Eberhart & Kennedy, (1995). It was developed by Eberhart & Kennedy, (1995), inspired by creatures such as birds and fish that move in flocks. It has been observed that creatures that move in flocks are more successful in hunting, finding rich food and hiding from dangers. The basis of the PSO algorithm is actually very similar to the method used by these animals. In the algorithm, there is a swarm of particles that make up this herd,

just like in a living community. To use the algorithm properly, the parameters to be optimized are first determined. Then, an objective function containing these parameters should be created. Values are determined to approximate the objective function. These values may be values such as literature data or experimental and test results. In order for the algorithm to quickly converge to the desired values, the possible upper and lower limit values of the parameters to be optimized are created by a small manual calculation. Thus, the range that the algorithm will predict is narrowed, which reduces the convergence time. According to the defined values, other particles are positioned according to the particle with the best position at the first moment of the swarm and the algorithm starts to work iteratively. If the target values are approached as a result of the first iteration, the swarm is positioned according to the last obtained value. This continues until the margin of error is lowest. In each iteration, the particles try to come to a better position than the previous one. Finally, when the iterations are completed, the best position of the relevant parameters between the specified upper and lower values is found.

The equation for updating the velocity of each particle i within the swarm at iteration t can be expressed as follows Equation (3.28) Freitas et al., (2020):

$$\vec{V}_{t+1}^{i} = \vec{V}_{t}^{i} + \varphi_1 R_{1t}^{i}\left(\vec{p}_{t}^{i} - \vec{x}_{t}^{i}\right) + \varphi_2 R_{2t}^{i}\left(\vec{g}_{t} - \vec{x}_{t}^{i}\right) \tag{3.29}$$

$$\vec{x}_{t+1}^{i} = \vec{x}_{t}^{i} + \vec{V}_{t+1}^{i} \tag{3.30}$$

In an alternative expression, φ_1 and φ_2 are actual acceleration coefficients referred to as cognitive and social weights. These coefficients determine the extent to which the particle's velocity and trajectory should be influenced by the global and individual best positions. R_1 and R_2 are d-dimensional random vectors distributed uniformly. Furthermore, $\vec{p}_t^{\,i}$ and $\vec{g}_t$ denote, in sequence, the personal or individual best position of particle i at iteration t and the prevailing global best position of the entire swarm.

The PSO algorithm Eberhart & Kennedy, (1995) was used to calculate the operating parameters of the ECHC. Table 3.2 shows the parameters calculated using the PSO algorithm.

Table 3. 2 The parameters found by using PSO algorithm.

Definition	**Unit**	**Upper Value**	**Lower Value**
Reference Change Current Density of Anode Side (i_{0a}^{ref})	A/m^2	85000	4000
Reference Change Current Density of Cathode Side i_{0c}^{ref}	A/m^2	100000	40000
Contact Resistance ($R_{contact}$)	$ohm \cdot m^2$	10^{-3}	10^{-5}
Activation Energy (E_a)	$kJ \cdot mol^{-1}$	18	13

3.3 Model Verification

This thesis focuses on mathematical modeling of Electrochemical Hydrogen Compression (ECHC) cells. Modeling results were compared with studies in the literature and confirmed with experimental results. Experimental studies were meticulously carried out by Atılım University, and within the scope of these studies, both purification and pressurization experiments were carried out.

In purification experiments, the performance of the ECHC cell using various mixed gases was examined in the temperature range between 140°C and 180°C. These studies have provided important data to understand the cell's responses under different operating conditions.

In the pressurization studies, first a single-cell ECHC cell was examined in detail. Then, a 5-cell ECHC cell was created and the performance parameters in this stack-cell system were evaluated. For detailed information about the experimental setup and procedures, the sources that form the basis of this study, especially the works of Durmuş, (2023) and Bulanık Durmuş et al., (2024) can be consulted.

This comprehensive study has devoted significant effort to advancing mathematical modeling of ECHC cells as well as verifying the agreement between experimental results and theoretical predictions. In this way, it makes a valuable contribution to the effective understanding and optimization of ECHC technology.

In this modeling approach, for the single cell of ECHC, the effect of back diffusion on the cell performance was examined. Since the highest efficiency was obtained when the cell voltage was kept constant at 0.075 V, this voltage value was preferred among the reference article Chouhan, Bahar, et al., (2020) values for the relevant calculations. In Figures 3.4-3.7 model outputs and reference article values are presented graphically. The variance between the outcomes generated by the model and the data reported in the literature was under 8%. This slight difference can be attributed to the inability to utilize the complete values from the literature data. In other words, the model results closely align with the available literature, and any disparities are primarily a result of the constraints in accessing the full set of values from the referenced data. This acknowledgment clarifies that the model's performance is generally in good agreement with the literature, considering the limitations in data accessibility.

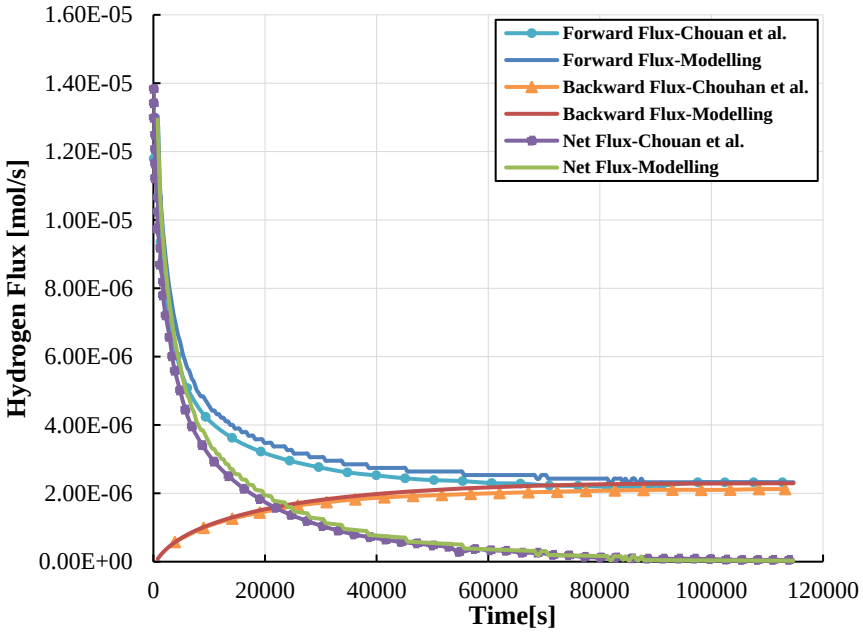

Figure 3. 4 Change of forward and backward H_2 molar flow rate over time at a constant cell voltage of 0.075 V

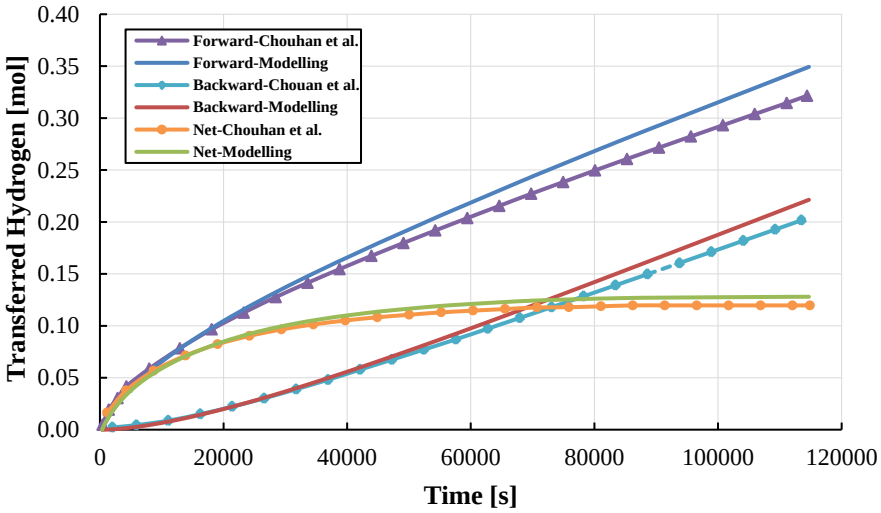

Figure 3. 5 Change of forward and backward transferred H_2 molar flow rate over time at a constant cell voltage of 0.075 V

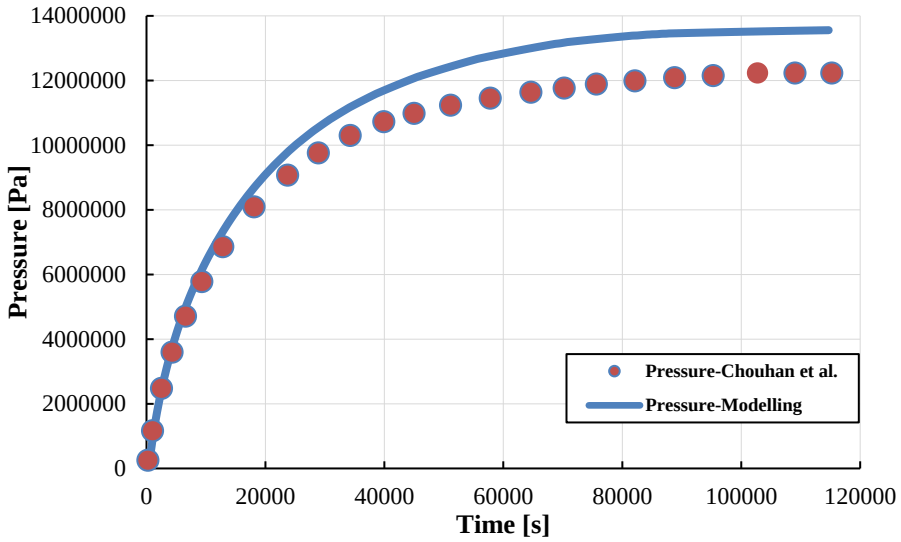

Figure 3. 6 Change of cathode pressure with time at a constant cell voltage of 0.075 V

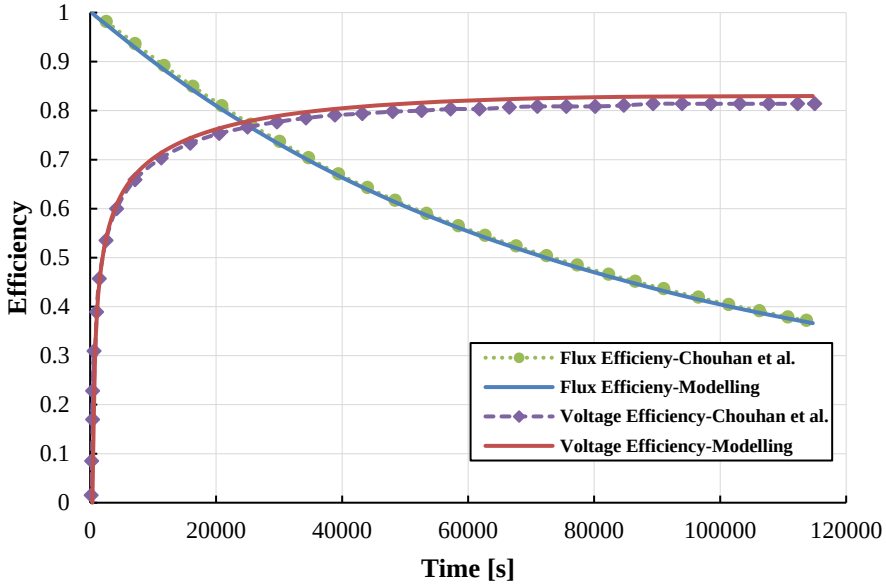

Figure 3. 7 Variation of ECHC cell current, voltage, and cell efficiency with time at a constant cell voltage of 0.075 V

3.4 Experimental Studies

In Electrochemical Hydrogen Compressor (ECHC) systems, it has been shown that operating at high temperatures (100°C and above) significantly improves the impurity tolerance of the cells. Therefore, the low carbon monoxide (CO) tolerance observed in ECHC systems operating at lower temperatures can be overcome by operating at higher temperatures. In particular, the impurity tolerance of the system increases significantly when operating in the temperature range of 140-200°C.

The experimental data used in the validation phase of this thesis was obtained by Bulanık Durmuş et al., (2024) from Atılım University. As part of this research, high-temperature single-cell ECHC systems and five-cell ECHC stacks were designed and manufactured to facilitate the separation of high-purity hydrogen (H_2) from reformate gas mixtures containing H_2, carbon dioxide (CO_2), and CO. In addition, extensive electrochemical experiments were conducted to purify and pressurize H_2 in these systems.

To optimize the hydrogen purification performance of ECHCs at high temperatures, composite membranes based on polybenzimidazole (PBI) and metal-organic frameworks (MOFs) have been developed. These materials were chosen due to their superior resistance to high temperatures. The preparation steps for PBI membranes are shown in Figure 3.8.

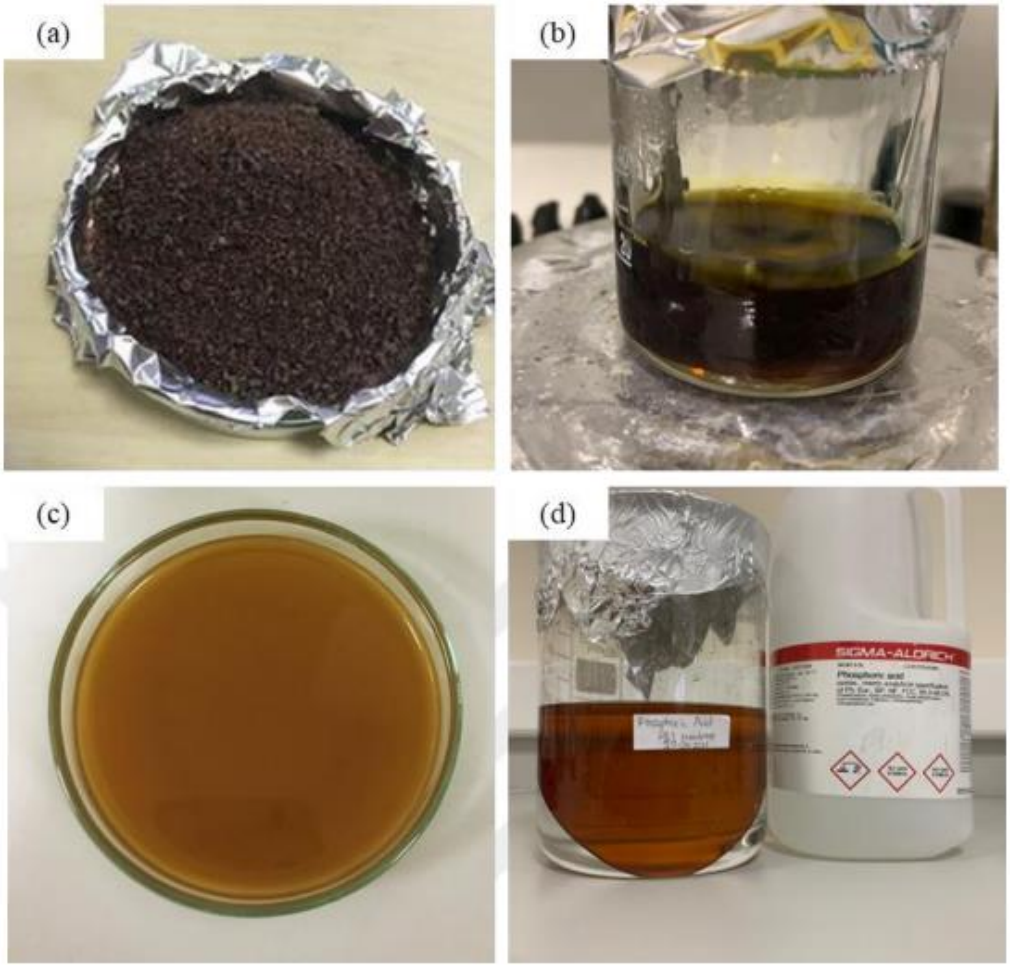

Figure 3. 8 PBI membrane preparation steps, Bulanık Durmuş et al., (2024)

Material of the synthesis of PBI polymer followed the procedure outlined in reference Bulanık Durmuş et al., (2024). The materials used were diaminobenzidine tetrachloride hydrate (DAB.4HCl.2H_2O, 98%), isophthalic acid (IPA, 99%), polyphosphoric acid (PPA, 115%), phosphoric acid (H_3PO_4, 85%), and N,N-dimethylacetamide (DMAc), all obtained from Sigma-Aldrich (USA).

The MEAs were prepared using the ultrasonic coating technique, which has proven effective in minimizing catalyst loss and ensuring a uniform coating. Initially, gas diffusion electrodes were prepared. These electrodes were then combined with the PBI-MOF membrane through hot pressing on both sides. To prepare the electrodes, a catalyst solution was first made by combining a Pt/C catalyst with a PVDF binder and isopropanol solvent. Using an ultrasonic coating device operating at 120 kHz and 80°C, the homogeneous catalyst mixture was applied to the commercial gas diffusion layer. The preparation steps of GDE are shown in Figure 3.9.

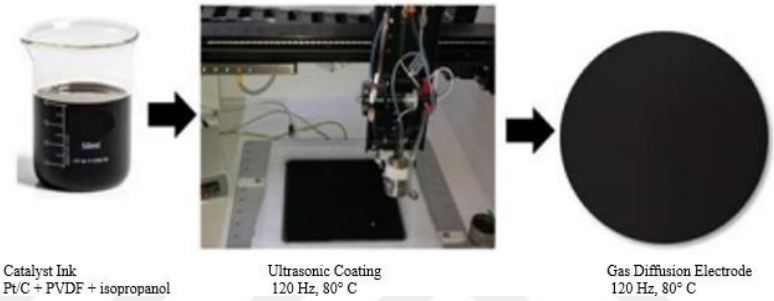

Figure 3. 9 GDE preparation steps, Bulanık Durmuş et al., (2024)

Finally, the prepared electrodes were cut according to the cell design and MEAs were prepared by hot pressing both surfaces of phosphoric acid impregnated membranes at 150° C and 172 N/cm^2 for 15 minutes. The preparation steps of MEA are shown in Figure 3.10.

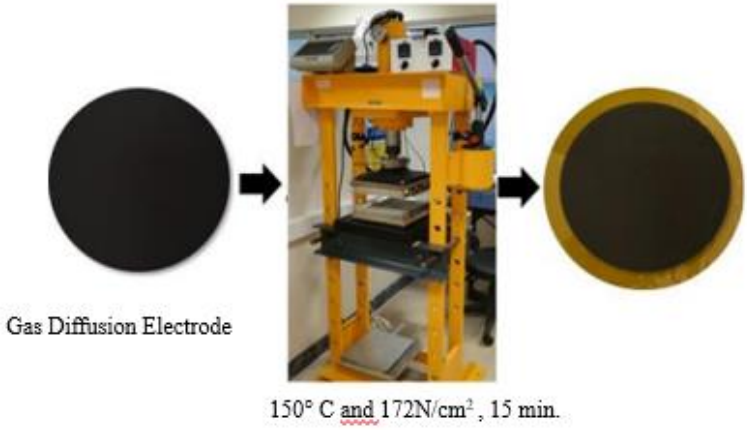

Figure 3. 10 MEA preparation steps, Bulanık Durmuş et al., (2024)

Figure 3.11 and Figure 3.12 illustrate the three-dimensional designs of the ECHC single cell and the five-cell ECHC stack components, respectively. In scope of the reference thesis, a five-cell ECHC stack was designed, maintaining the same active area as the single ECHC cell. The components for this stack were subsequently prepared. The five-cell ECHC stack retains the identical cell design as the single-cell ECHC.

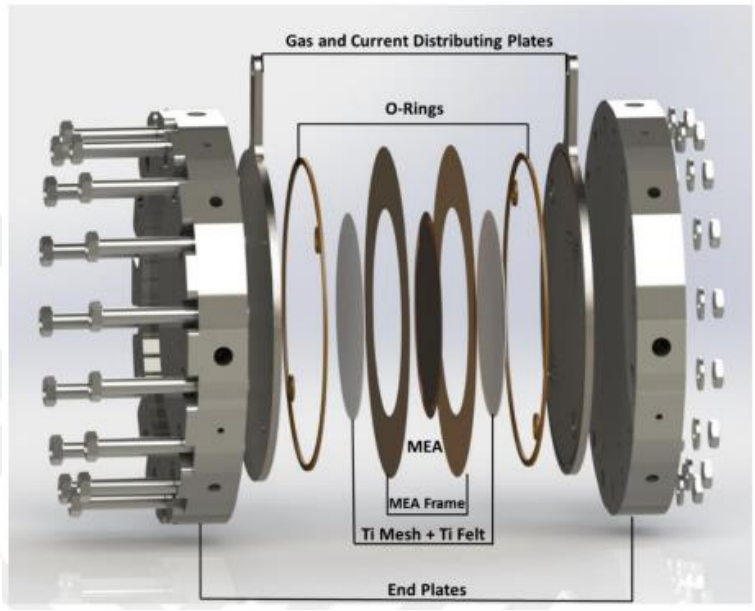

Figure 3. 11 Single-cell HT-ECHC, Bulanık Durmuş et al., (2024)

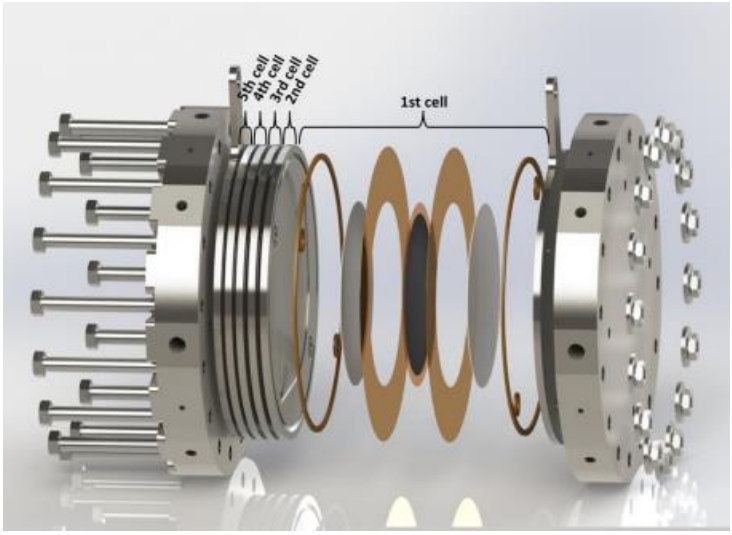

Figure 3. 12 Stack level (5 cell) HT-ECHC, Bulanık Durmuş et al., (2024)

Figure 3.13a and Figure 3.13b present the assembled of the single cell and the five-cell ECHC stack, respectively.

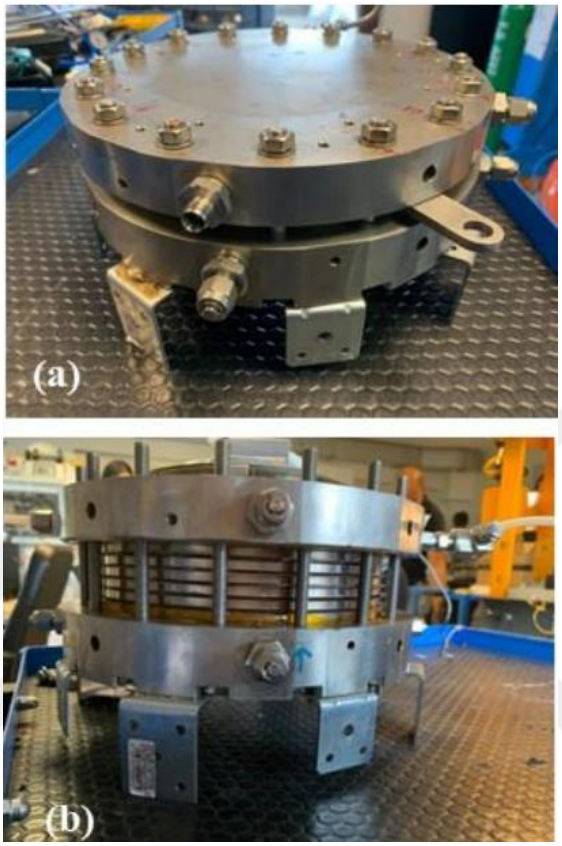

Figure 3. 13 The assembled HT-ECHC single cell and stack, Bulanık Durmuş et al., (2024)

For conducting high-temperature ECHC purification tests, an experimental setup was established. This setup included various components such as tubes for H_2, a reformate gas mixture, and nitrogen gases. Additionally, micro-flow controllers, a power generator, back pressure regulators, a frequency response analyzer, and a computer with specialized software to control the entire system were integrated. The detailed arrangement of this setup is illustrated in Figure 3.14.

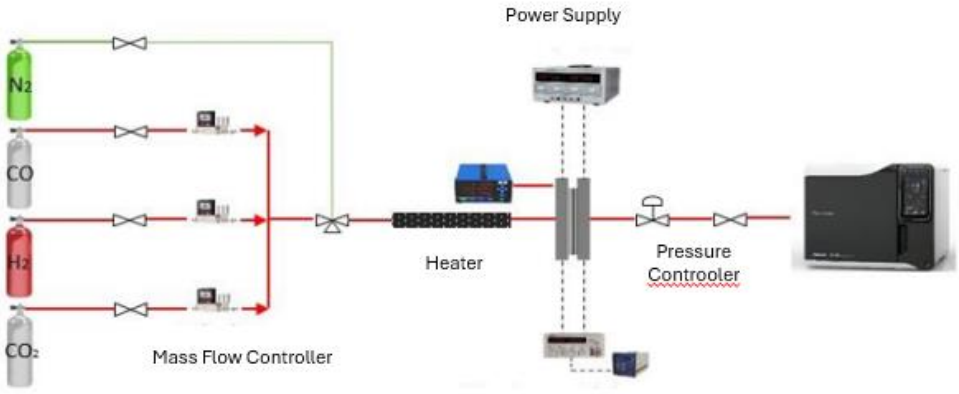

Figure 3. 14 HT-ECHC purification test setup flow diagram, Bulanık Durmuş et al., (2024)

The experimental setup used for testing the HT-ECHC cell's performance is shown in Figure 3.15. Pressurization tests were done with an ECHC cell that has a 100 cm² active area, at a temperature of 160°C, using pure hydrogen (99.999%). The test station included a digital mass flow controller (Alborg) to adjust the gas flow rate, a pressure gauge to monitor pressure, and a DC power supply to provide the necessary electricity.

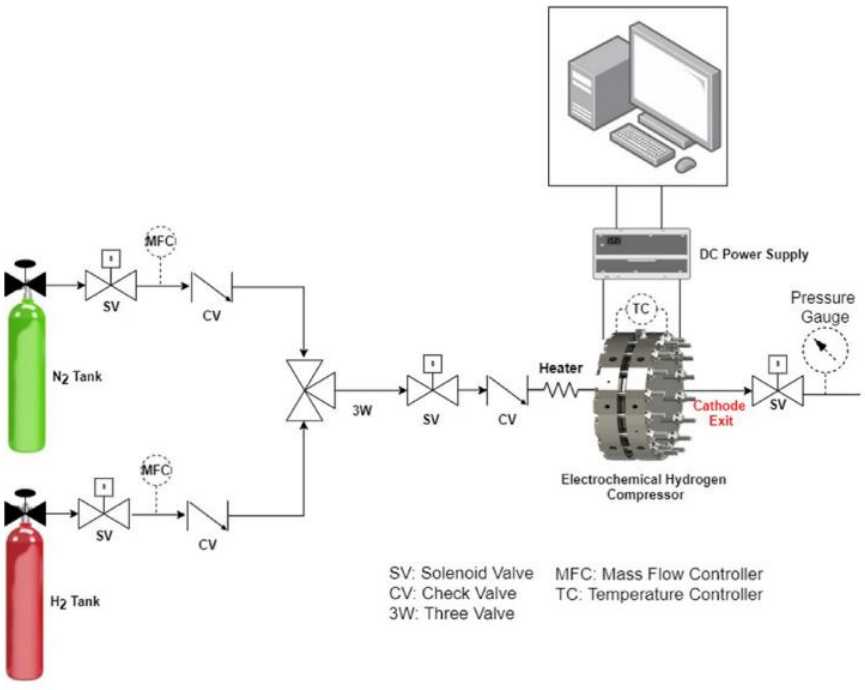

Figure 3. 15 HT-ECHC performance test system, Bulanık Durmuş et al., (2024)

The main focus of this thesis is on modeling studies, detailed experimental methodologies and results can be found in the referenced work Bulanık Durmuş et al., (2024).

CHAPTER FOUR
RESULTS AND DISCUSSION

4.1 Operation with Pure H_2 Feeding

Several parameters have a substantial impact on the performance of the ECHC cell, encompassing factors such as temperature, membrane type and thickness, catalyst type, and the purity level of the feed gas. Among these parameters, operating temperature stands out as the parameter that affects the performance of the ECHC cell significantly. The main reason for this effect is that temperature increases the reaction kinetics. Although an increase in the operating temperature increases the conductivity of the membrane and has a positive effect on cell performance, if the temperature exceeds a certain value, it damages the membrane strength. For this reason, working at an optimum temperature is very important to achieve maximum performance and durability.

In this study, the electrochemical reaction was carried out at 140°C-180°C and pure H_2 supply, while the anode side was kept under atmospheric pressure. Since pure H_2 gas enters from the anode section, the pressure of the anode and cathode section is taken as equal to 1 atm. As can be seen in Figure 4, considering a constant cell voltage, the largest corresponding current density occurs at a temperature condition of 160°C. Feeding with pure H_2 gas showed a profile very close to linear in the graphics. The reason why the current density-voltage curve has a linear profile is explained by the fact that the primary factor influencing the cell voltage during the reaction is the ohmic voltage. It can be seen from the equations explained under the heading 3.1.1 that the relation between ohmic voltage equation and and current density is linear.

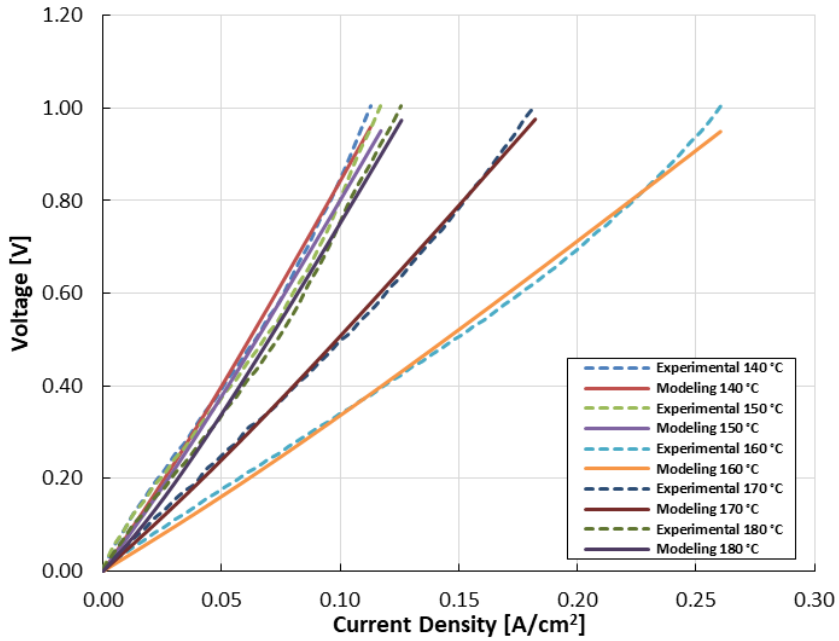

Figure 4. 1 Experimental and modelling results of pure H_2 gas between 140°C-180°C temperatures

4.2 Operation with Feeding Reformate Gas Mixtures

The results obtained for 5 different temperature values when the H_2/CO_2 mixture gas is fed to the compressor with a ratio of (0.75:0.25) and a flow rate of 0.25 (slpm), respectively, are shown in Figure 4.2. In the modeling, verification of experimental data between 0 and 0.7 V values was carried out. Based on these findings, it becomes evident that both experimental and modeling studies exhibit a linear pattern within these ranges, mirroring the behavior observed during pure hydrogen feeding. When the results were examined, the highest current density values were obtained in the 160°C curve, as in the values obtained with pure H_2 feeding. As mentioned before, cell efficiency decreased if a certain temperature value was exceeded. As can be seen from Figure 4.2, a lower performance was observed at 170°C and 180°C, which exceeded 160°C.

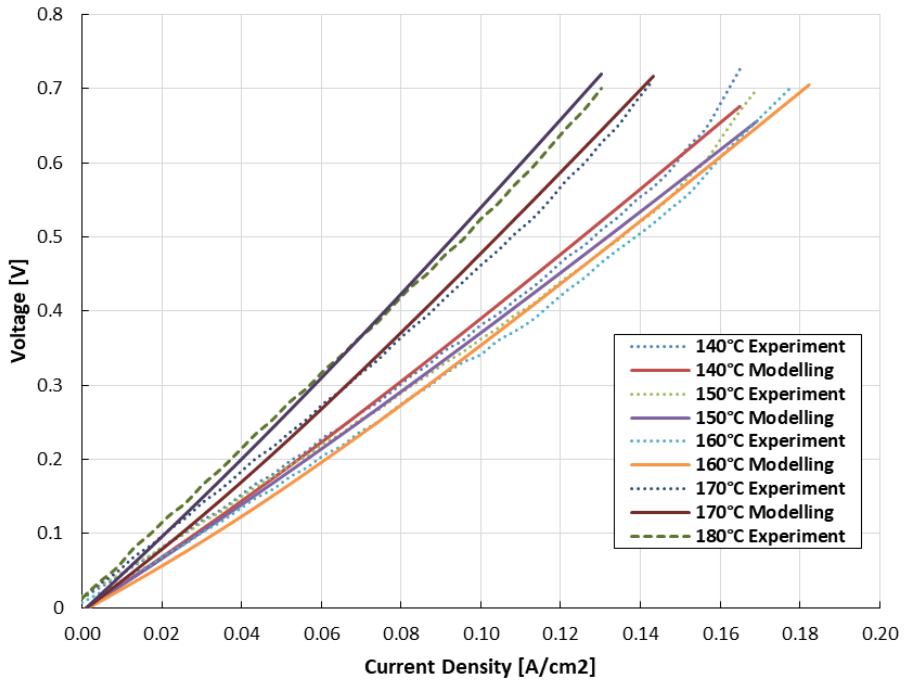

Figure 4. 2 Experimental and modeling results of H_2/CO_2 (0.75:0.25) gas mixture between 140°C-180°C temperatures

The experimental and modeling results presented in Figure 4.3 show the behavior of the $H_2/CO_2/CO$ gas mixture (in composition 0.73:0.26:0.02, respectively) over the temperature range of 140°C to 180°C at a flow rate of 0.25 standard litres/min. Unlike the above-mentioned gas condition, CO gas was added to the mixture gas, and this resulted in a different result from the analysis performed with H_2/CO_2 and pure H_2 feeding. When the results are examined for a constant voltage value, it was seen that the current density increased again with the increase in temperature. However, unlike Figures 4.1 and 4.2, in this graph, although there is no significant difference compared to the curve obtained at 160 C, the most efficient curve was obtained at 180 C. It is thought that this situation is caused by the decrease in the active area of the plates due to poisoning caused by reformate gas. High temperature working conditions reduce poisoning. In addition, the voltage values resulting from the increase in current density lost their linear appearance after a certain point, unlike the previous cases. So, it can be said that activation overvoltage and Nernst voltage become dominant here.

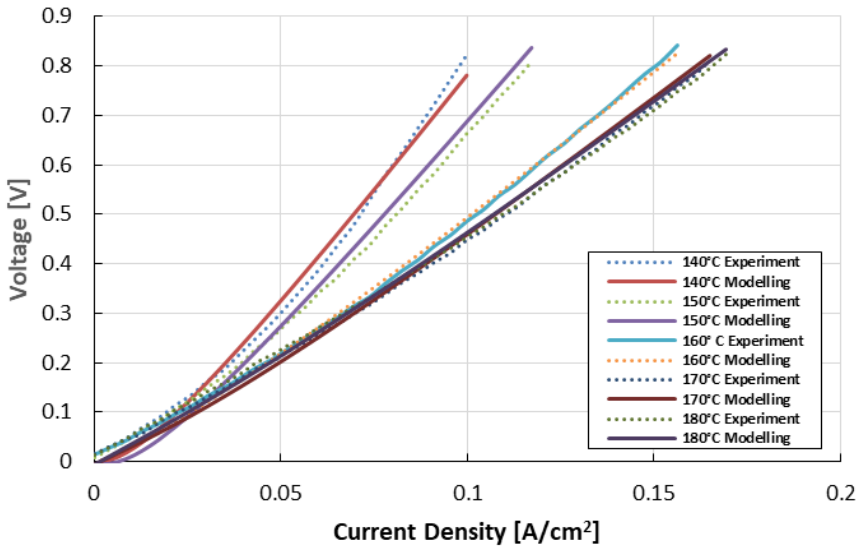

Figure 4. 3 Experimental and modeling results of $H_2/CO_2/CO$ (0.73:0.26:0.02) gas mixture between 140°C-180°C temperatures

In Figures 4.4 and 4.5, current and voltage curves obtained with the H_2/CO feed gas mixing ratio of (0.95:0.05), (0.97:0.03) and 0.25 (slpm) flow rate are shown, respectively. The results from both graphs indicate a close resemblance. Moreover, it is evident that reducing the proportion of CO gas in the mixture enhances the current density obtained at the same voltage for temperatures of 140°C, 150°C, and 160°C.

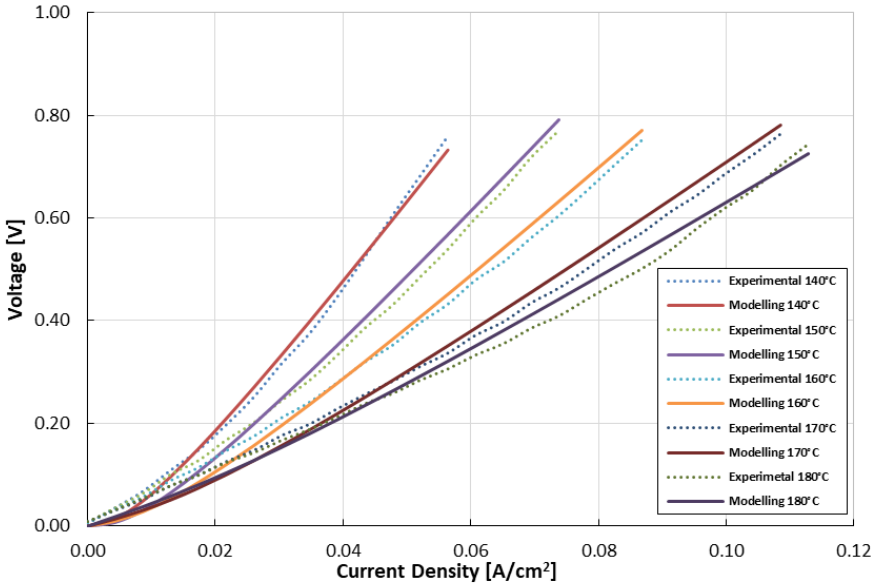

Figure 4. 4 Experimental and modeling results of H_2/CO (0.95:0.05) gas mixture between 140°C-180°C temperatures

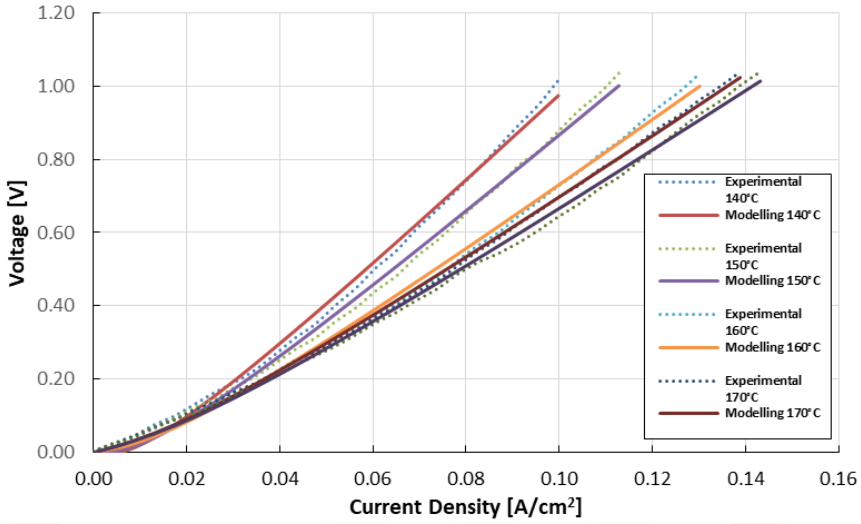

Figure 4. 5 Experimental and modeling results of H_2/CO (0.97:0.03) gas mixture between 140°C-180°C temperatures

4.3 Comparison and Interpretation of the Efficiencies of the Results Obtained at Different Ratios of Mixing Gas

When the results of the mixture of H_2CO gas in different proportions were examined, the voltage required for the same current value was examined. The ECHC cell was fed with H_2CO gas, featuring mixing ratios of 0.97:0.03 and 0.95:0.05. When the polarization curves obtained from gas mixtures were examined, it was observed that at equivalent cell voltages, the current density in the mixture with reduced CO content constantly exceeded that of the other mixture. This means that the cell works more efficiently at that mixing ratio. It is thought that the reason for this is that as the amount of CO increases, the rate of poisoning of the catalysts increases. It has been seen that the efficiency increases with the increase in temperature. It was observed that the most efficient results were obtained at 180 º C.

4.4 Effect of Back Diffusion at Constant Cell Voltage (Single Cell)

The compression tests were conducted while taking the cell voltage as constant (0.1 V, 0.2 V, 0.4 V, 0.6 V, 0.8 V, 1 V, and 1.5 V). During these tests, the current values that the HT-ECHC cell drew from the power source were recorded as illustrated in

Figure 4.6. The current values occurring at each cell voltage were used to calculate the forward and backward H_2 molar flow rate occurring at that cell voltage Bulanık Durmuş et al., (2024).

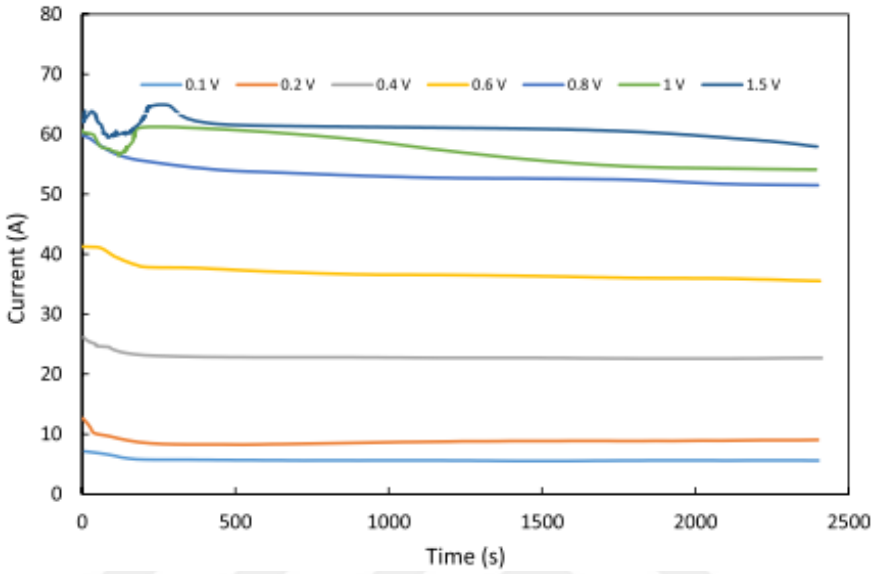

Figure 4. 6 Variation of current with time at different operating cell voltages

4.4.1 Investigation of the Change of Forward and Backward H_2 Molar flow rate with Time at Different Cell Voltage Values

The change of H_2 molar flow rate across the membrane with time during the ECHC pressurization process was examined for different cell voltages. The forward molar flow rate is obtained from Equation (3.8). It can be seen from Figure 4.7 that the forward H_2 molar flow rate decreases rapidly with time at the beginning of the compression process and remains constant after a while.

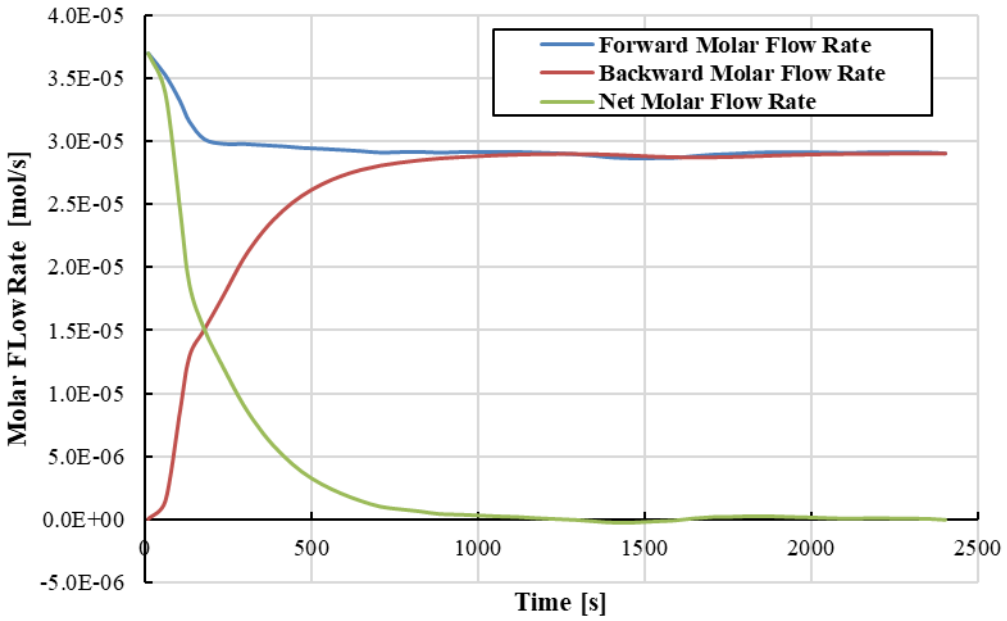

Figure 4. 7 Change of forward and backward H_2 molar flow rate over time at a constant cell voltage of 0.1 V

The backward molar flow rate is obtained using Equation (3.9). As can be seen in Figure 4.7, while the backward molar flow rate was initially 0 due to the lack of effect of backward diffusion, it increased rapidly over time and reached equilibrium after a certain period, as in the forward molar flow rate. When both molar flow rates reach equilibrium, the net H_2 molar flow rate across the membrane reduces to zero, and at the same time the cathode pressure reaches equilibrium. According to the results obtained, the forward H_2 molar flow rate was determined as $3x10^{-5}$ mol/s at a constant 0.1 V cell voltage.

The results obtained at a constant cell voltage of 0.2 V are given in Figure 4.8. An increase in forward H_2 molar flow rate was determined at 0.2 V cell voltage. The increase in forward H_2 flow resulted in an increase in the amount of H_2 transferred from the membrane and therefore an increase in the cathode pressure. It was observed that at this cell voltage, the forward H_2 molar flow rate increased to $4.58x10^{-5}$ mol/s.

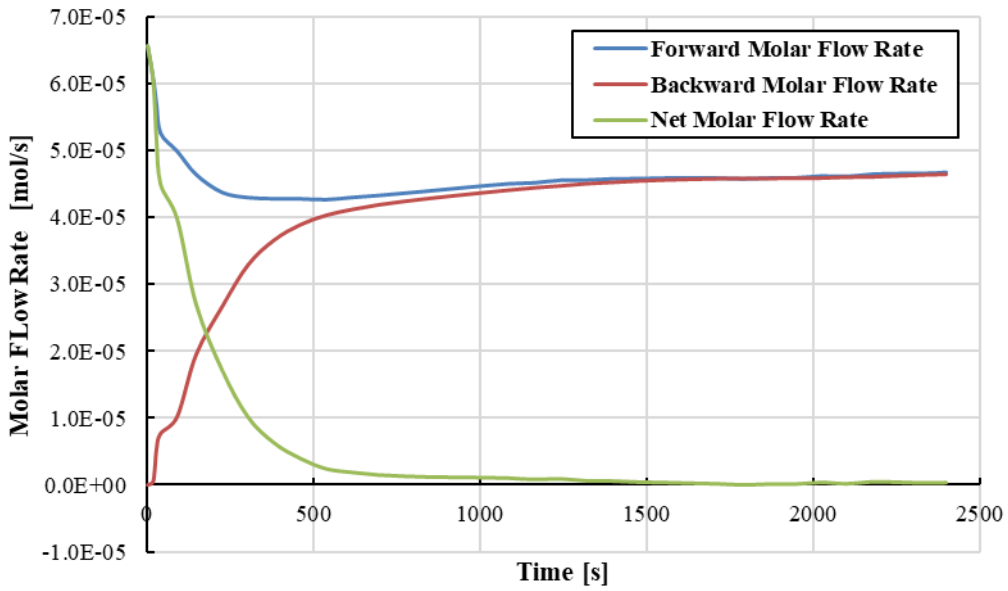

Figure 4. 8 Change of forward and backward H_2 molar flow ratees over time at a constant cell voltage of 0.2 V

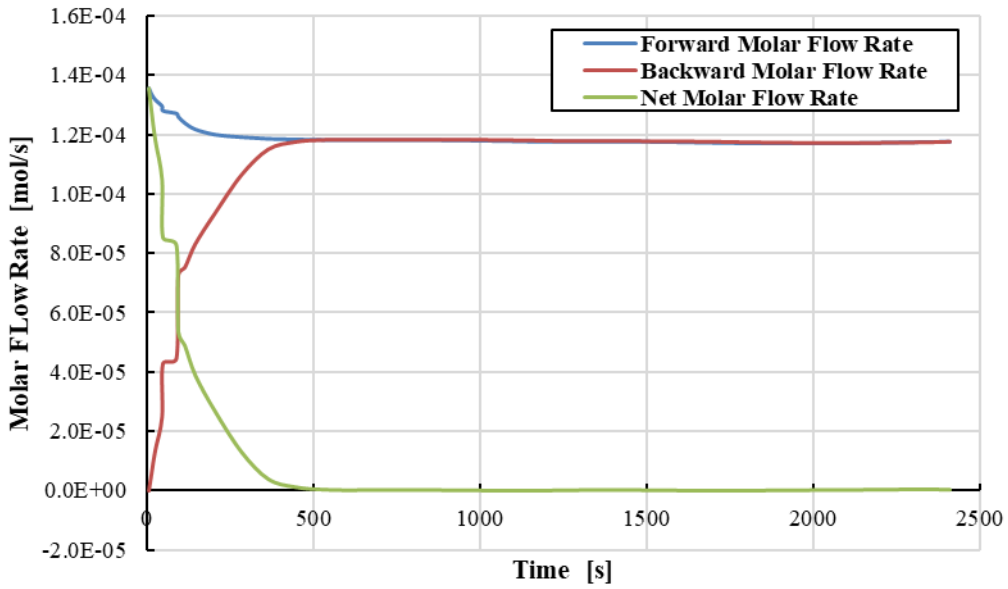

Figure 4. 9 Change of forward and backward H_2 molar flow rate over time at a constant cell voltage of 0.4 V

Figure 4.9 shows the molar flow rate results obtained at a constant cell voltage of 0.4 V. At a cell voltage of 0.4 V, the forward H_2 molar flow rate was determined as $1.2x10^{-4}$ mol/s. It was observed that there was an increase in the forward H_2 molar flow rate value obtained compared to the H_2 forward molar flow rate obtained at 0.2 V cell

voltage. Increasing the forward H_2 flow causes the amount of H_2 transferred from the membrane to increase and the cathode pressure to increase.

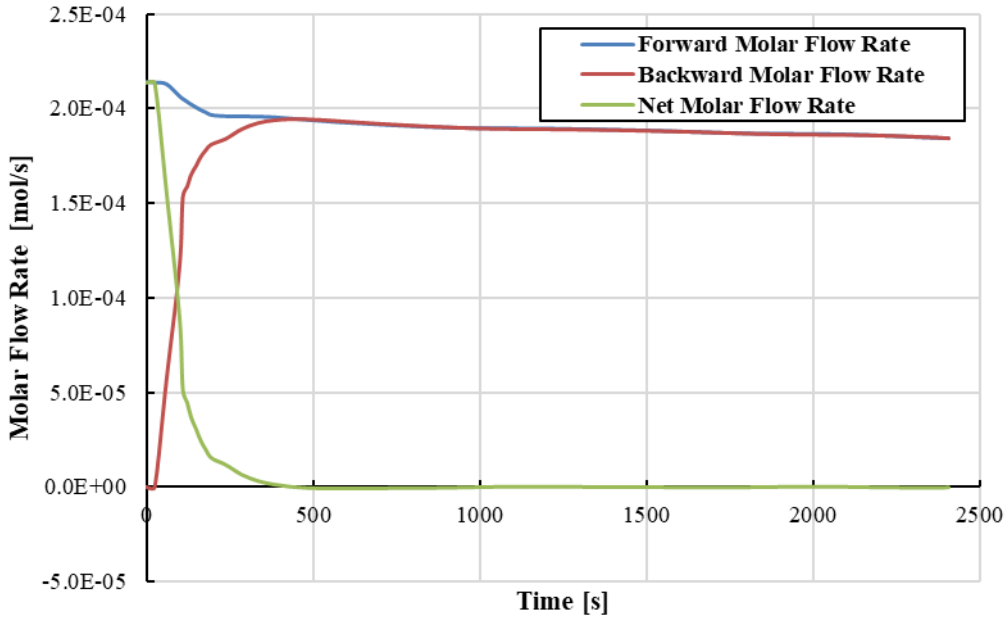

Figure 4. 10 Change of forward and backward H_2 molar flow rate over time at a constant cell voltage of 0.6 V

From Figure 4.10, it was determined that the forward H_2 molar flow rate was $1.8x10^{-4}$ mol/s at a constant cell voltage of 0.6 V. Increasing the forward H_2 flow causes the amount of H_2 transferred from the membrane to increase, thus causing the cathode pressure to be higher.

Figure 4.11 shows the change of forward and backward H_2 molar flow rate over time at a constant cell voltage of 0.8 V. It was observed that by increasing the cell voltage to a constant cell voltage of 0.8 V, the forward H_2 molar flow rate increased as expected, reaching $2.7x10^{-4}$ mol/s.

Figure 4.12 and Figure 4.13 show the changes with time of forward and backward H_2 molar flow rate for 1 V and 1.5 V cell voltages, respectively. Forward H_2 molar flow rates were determined as $2.81x10^{-4}$ mol/s and $3x10^{-4}$ mol/s for 1 V and 1.5 V cell voltages, respectively. It is seen that the forward H_2 molar flow rate increases with increasing cell voltage at both operating voltages. However, some initial fluctuations

were detected in the 1 V and 1.5 V cell operating voltages. These fluctuations are thought to be caused by fluctuations in the current drawn from the power supply due to the ohmic resistances the cell encountered during the experiment.

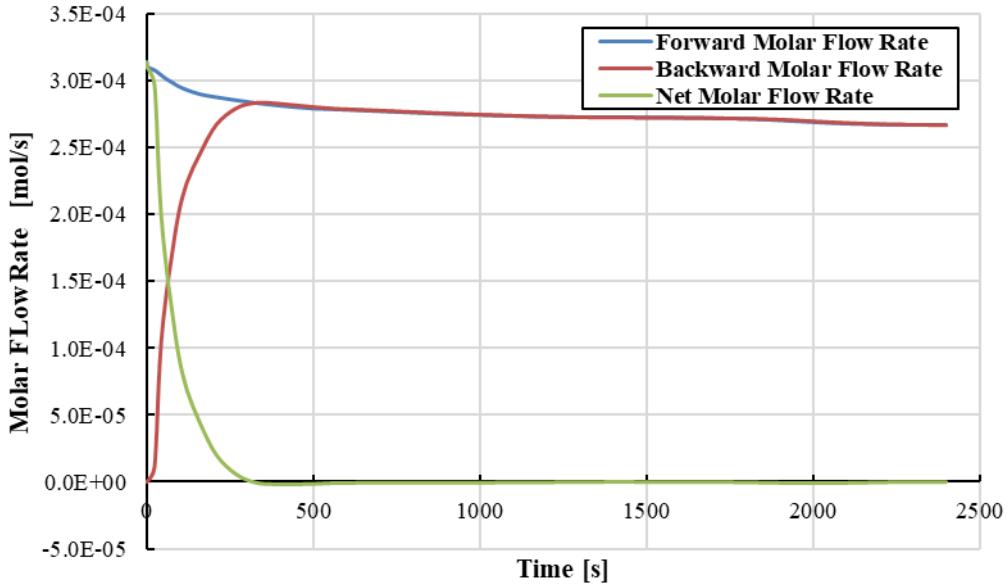

Figure 4. 11 Change of forward and backward H_2 molar flow rate over time at a constant cell voltage of 0.8 V

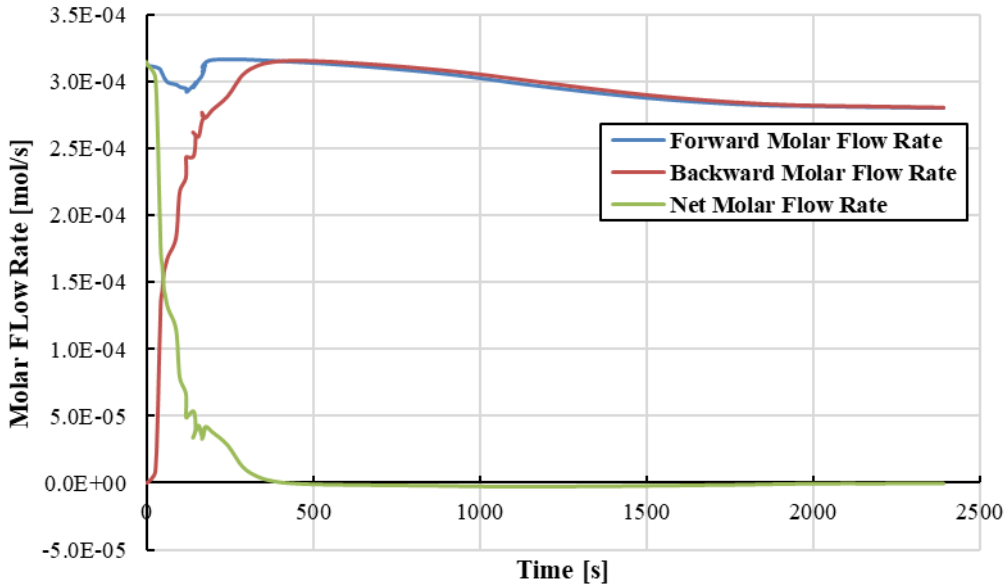

Figure 4. 12 Change of forward and backward H_2 molar flow rate over time at a constant cell voltage of 1 V

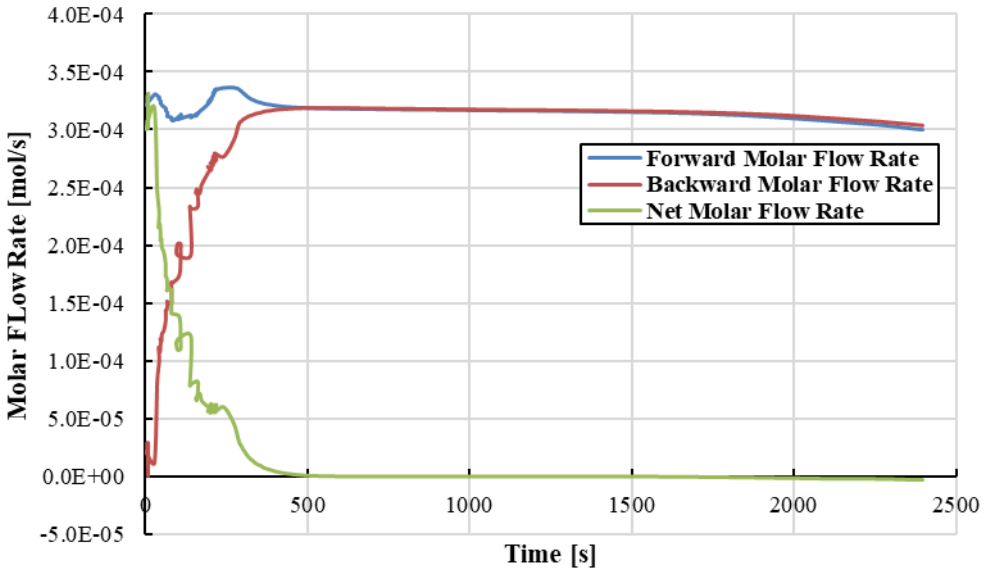

Figure 4. 13 Change of forward and backward H_2 molar flow rate over time at a constant cell voltage of 1.5 V

4.4.2 Investigation of the Change of the Amount of H_2 Transferred with Time at Different Cell Voltage Values

Figure 4.14 shows the change in the amount of H_2 transferred over time for a constant cell voltage of 0.1 V. For a fixed cell operating voltage of 0.1 V, the net amount of H_2 accumulated at the cathode was determined to be 0.0067 mol.

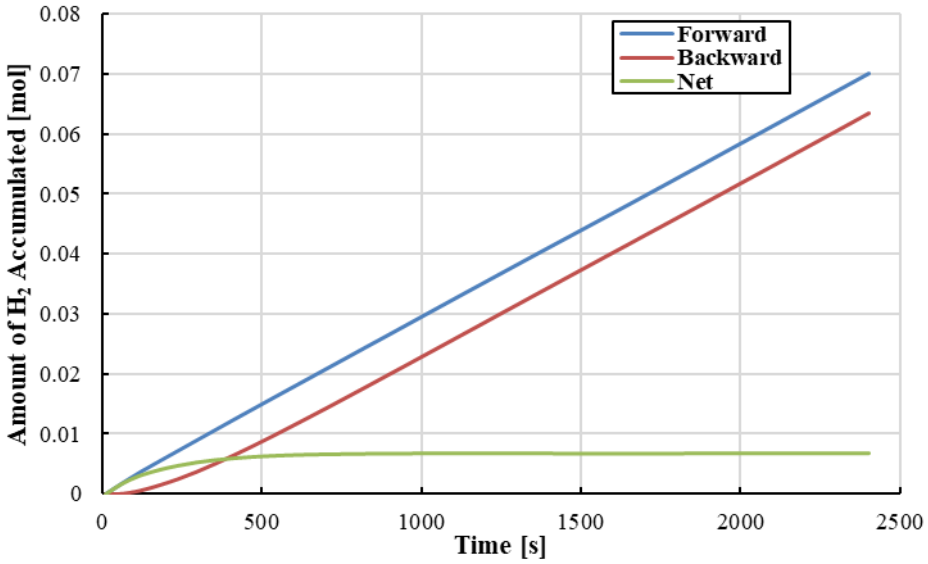

Figure 4. 14 Change of H_2 value transferred over time at 0.1 V constant cell voltage

In Figure 4.15, it is observed that when the cell operating voltage is increased to 0.2 V, the accumulated net amount of H_2 increases and this value is around 0.00968 mol. The change of the net amount of H_2 accumulated over time at a constant cell voltage of 0.4 V is shown in Figure 4.16. It was observed that the accumulated net amount of H_2 increased with increasing cell voltage, as expected, and this value was around 0.0133 mol.

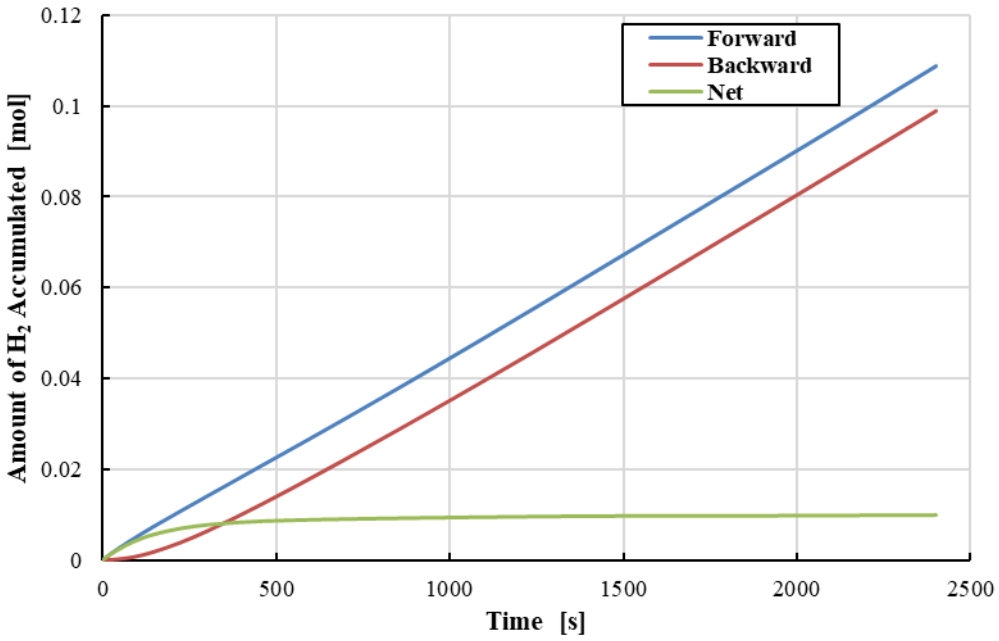

Figure 4. 15 Change of H_2 value transferred over time at 0.2 V constant cell voltage

Figure 4.17 shows the change in the net amount of H_2 transferred over time at a constant cell voltage of 0.6 V. As expected, it was determined that the accumulated net amount of H_2 increased with increasing cell operating voltage and this value was around 0.0174 mol. Figure 4.18, Figure 4.19 and Figure 4.20 show the net H_2 accumulated at constant cell voltages of 0.8 V, 1 V and 1.5 V, respectively. According to the results obtained, it was determined that since the H_2 molar flow rate reached the highest value at the highest cell voltage, the net amount of accumulated H_2 also reached the highest value.

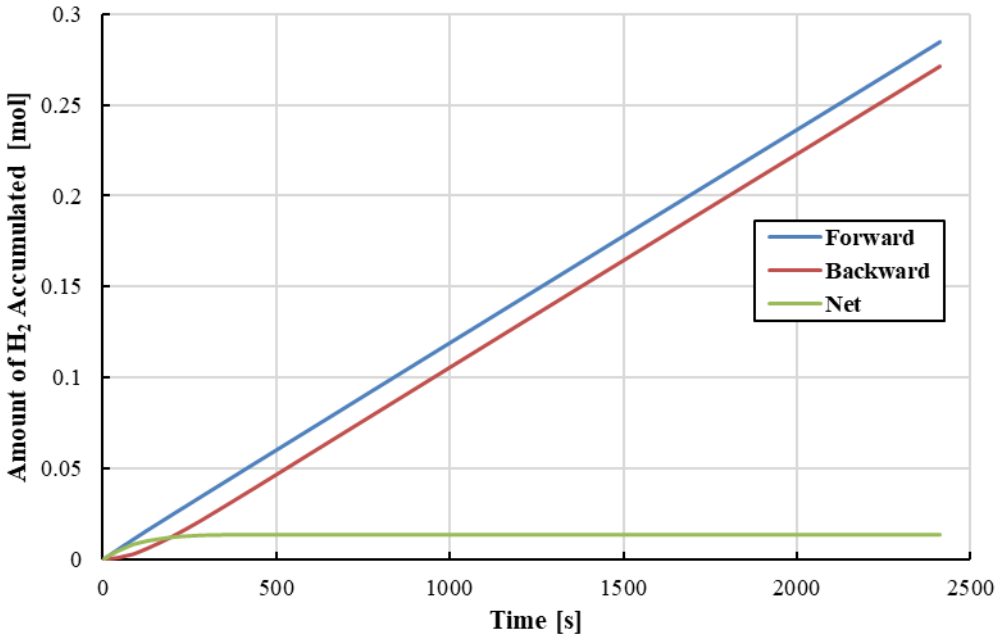

Figure 4. 16 Change of H_2 value transferred over time at 0.4 V constant cell voltage

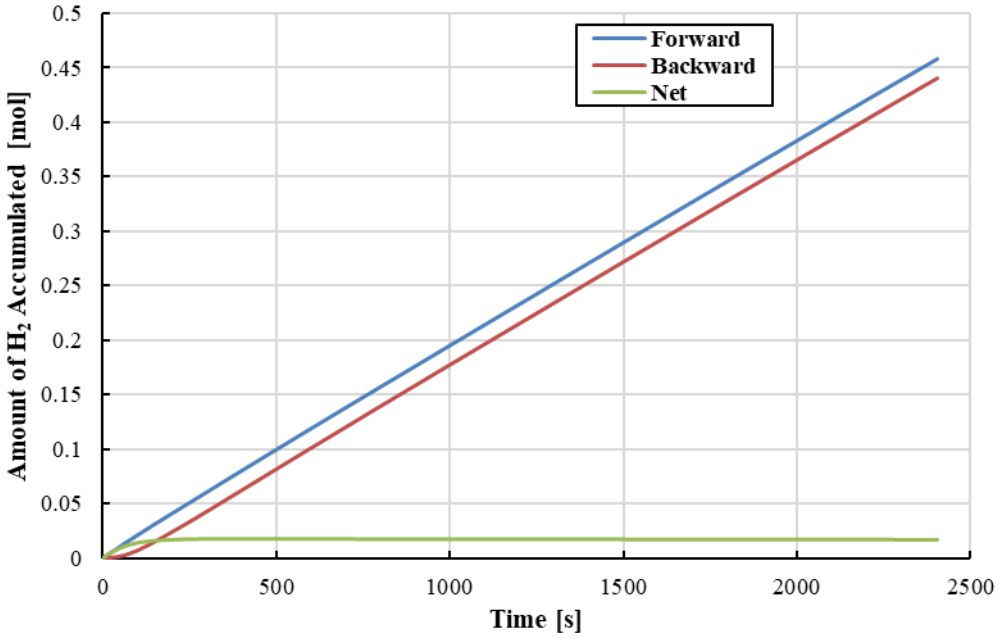

Figure 4. 17 Change of H_2 value transferred over time at 0.6 V constant cell voltage

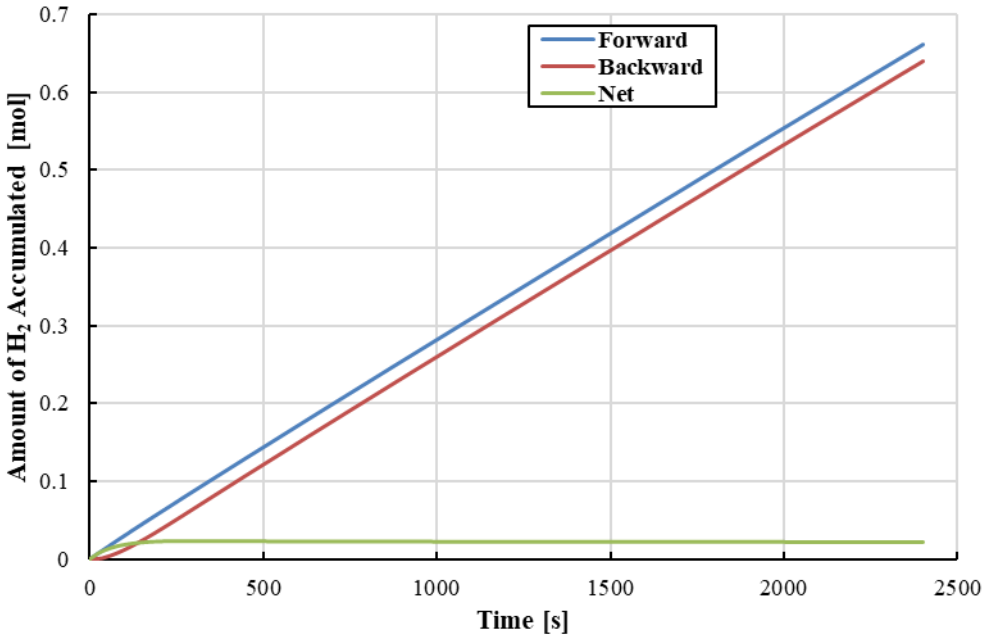

Figure 4. 18 Change of H_2 value transferred over time at 0.8 V constant cell voltage

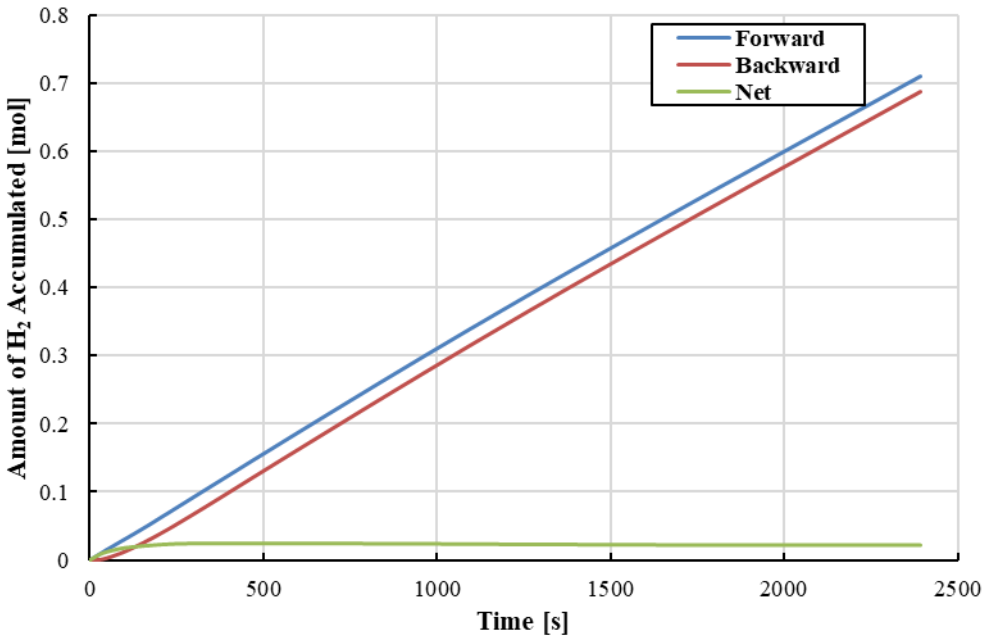

Figure 4. 19 Change of H_2 value transferred over time at 1 V constant cell voltage

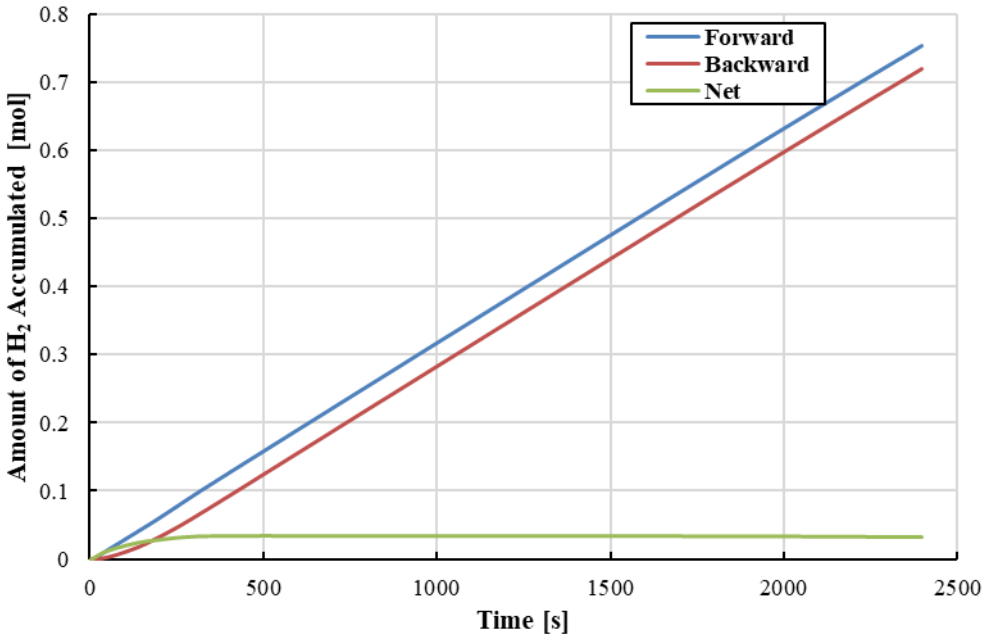

Figure 4. 20 Change of H_2 value transferred over time at 1.5 V constant cell voltage

4.4.3 Investigation of Pressure Values Obtained at Different Cell Voltage Values and Validation with Experimental Data

Modeling and experimental pressurization results are given comparatively in Figure 4.21. As can be seen from the figure, the model and experimental results are in perfect agreement. Initially, the cathode part has atmospheric pressure, as does the anode part. However, it was observed that as the H_2 molar flow rate increased, the net molar flow rate also increased. When Figure 4.21 is examined, it is determined that the amount of H_2 accumulated in the cathode section has a beneficial impact on pressure, the cathode pressure, which was initially at 1 bar, gradually increased and reached 11 bar, and the net molar flow rate remained constant as it reached equilibrium.

In Figure 4.22, the change of cathode pressure with time for a constant cell voltage of 0.2 V is shown comparatively for modeling and experimental results. When the results obtained are examined, it can be seen that the modeling and experimental results are in very good agreement, as in the case of a constant cell voltage of 0.1 V. It was observed that as the cell voltage was increased to 0.2 V, the pressure value increased and reached 15 bar. It is seen that the pressure stabilizes after approximately 1600 seconds as the flow stabilizes.

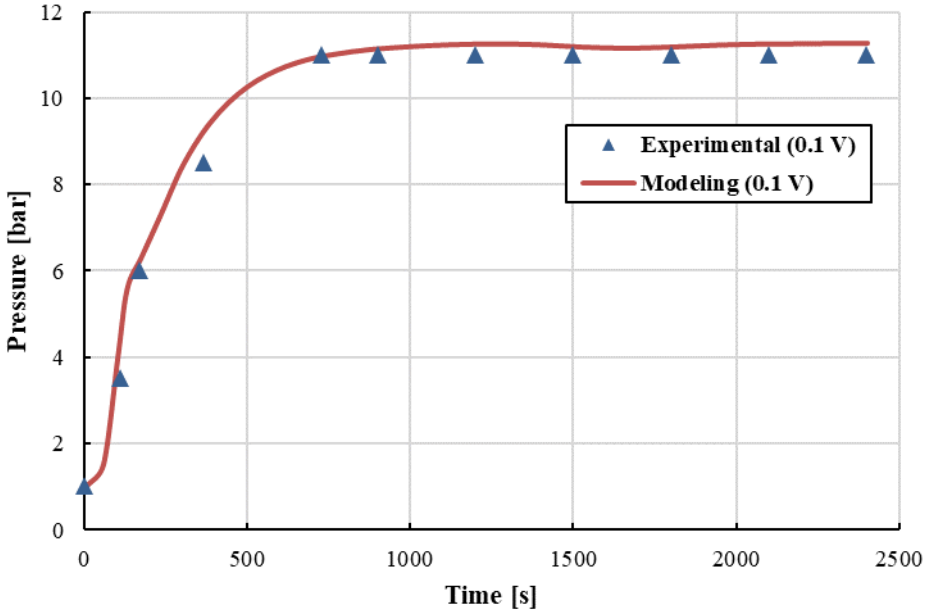

Figure 4. 21 Change of cathode pressure with time at a constant cell voltage of 0.1 V

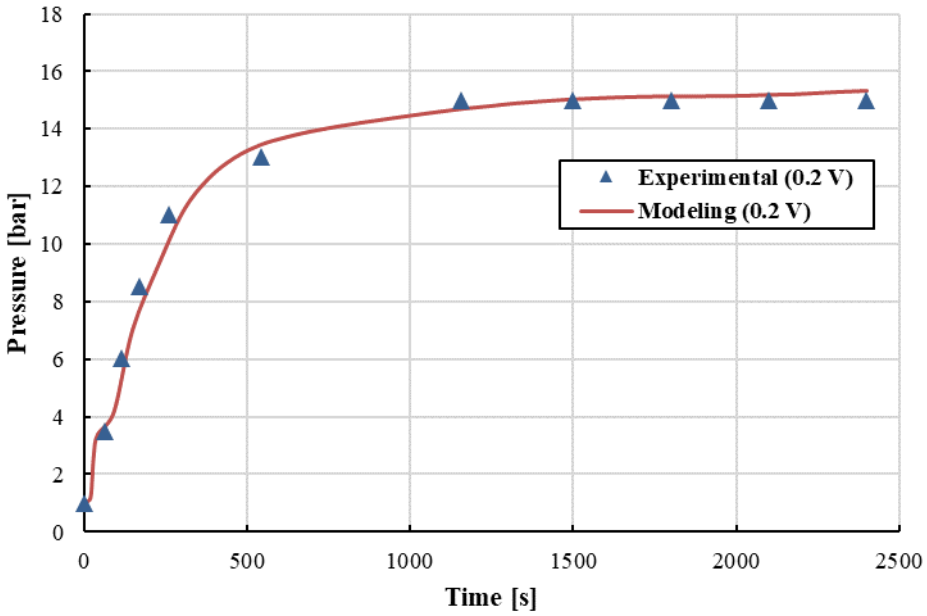

Figure 4. 22 Change of cathode pressure with time at a constant cell voltage of 0.2 V

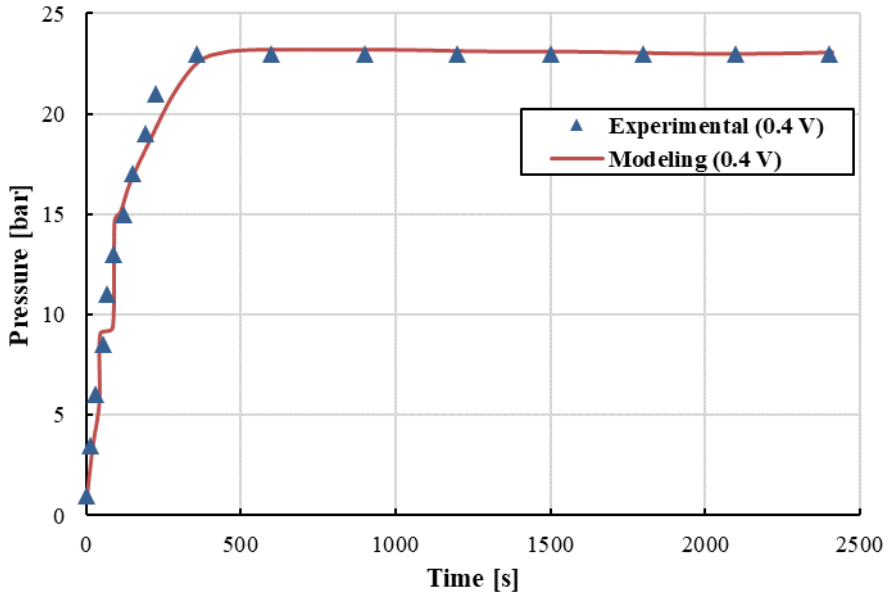

Figure 4. 23 Change of cathode pressure with time at a constant cell voltage of 0.4 V

The cathode pressure results obtained by increasing the cell operating voltage to 0.4 V are presented in Figure 4.23. When Figure 4.23 is examined, it is determined that the amount of H_2 accumulated in the cathode section positively influences the pressure, the cathode pressure, which was initially at 1 bar, gradually increased and reached 23 bar, and the net molar flow rate remained constant as it reached equilibrium.

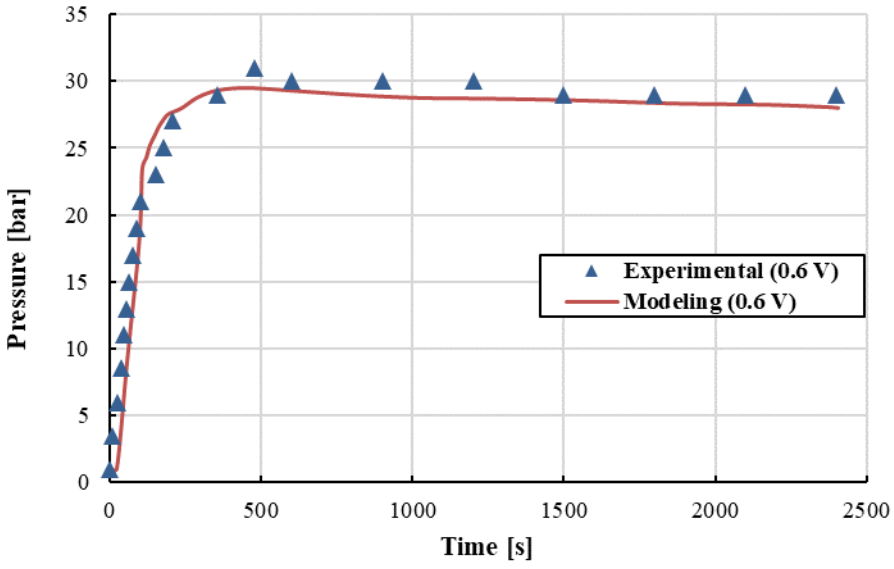

Figure 4. 24 Change of cathode pressure with time at a constant cell voltage of 0.6 V

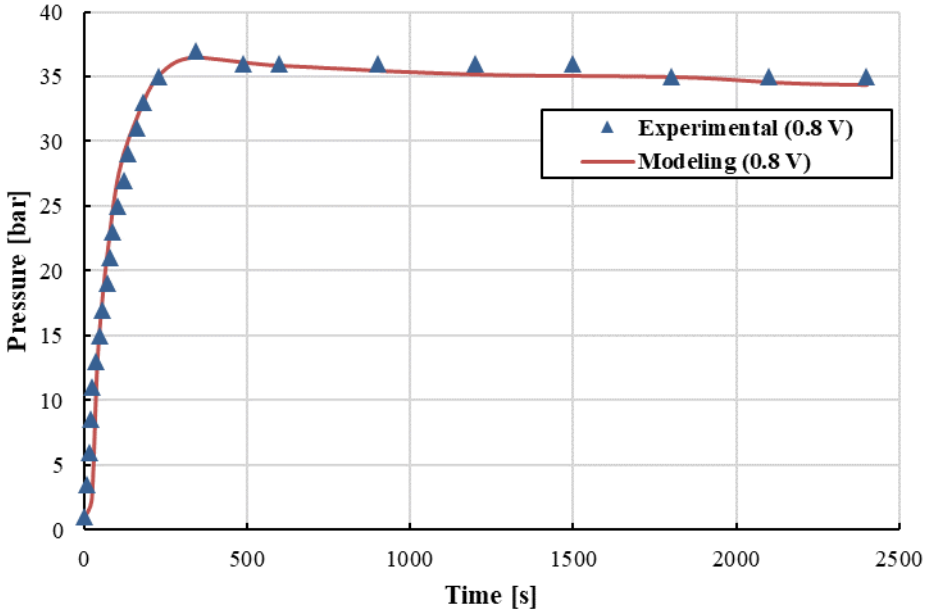

Figure 4. 25 Change of cathode pressure with time at a constant cell voltage of 0.8 V

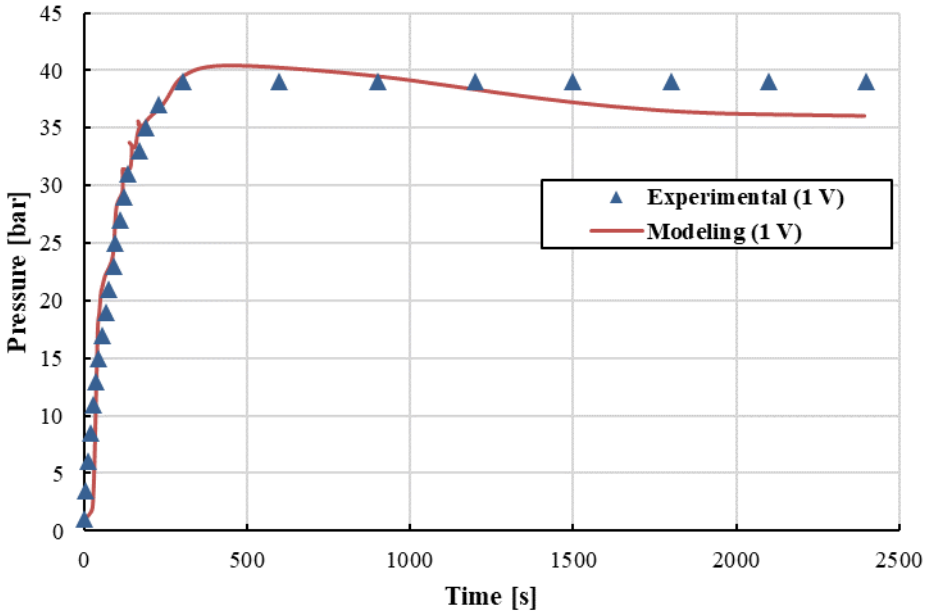

Figure 4. 26 Change of cathode pressure with time at a constant cell voltage of 1 V

The change of cathode pressure with time for constant cell operating voltages of 0.6 V, 0.8 V, 1 V and 1.5 V is given in Figure 4.24, Figure 4.25, Figure 4.26, and Figure 4.27, respectively. It has been determined that the model results obtained at all operating voltages are in very closely aligns with the experimental results. Cathode

pressures of 28 bar, 35 bar, 38 bar and 60 bar were reached for operating voltages of 0.6 V, 0.8 V, 1 V and 1.5 V, respectively.

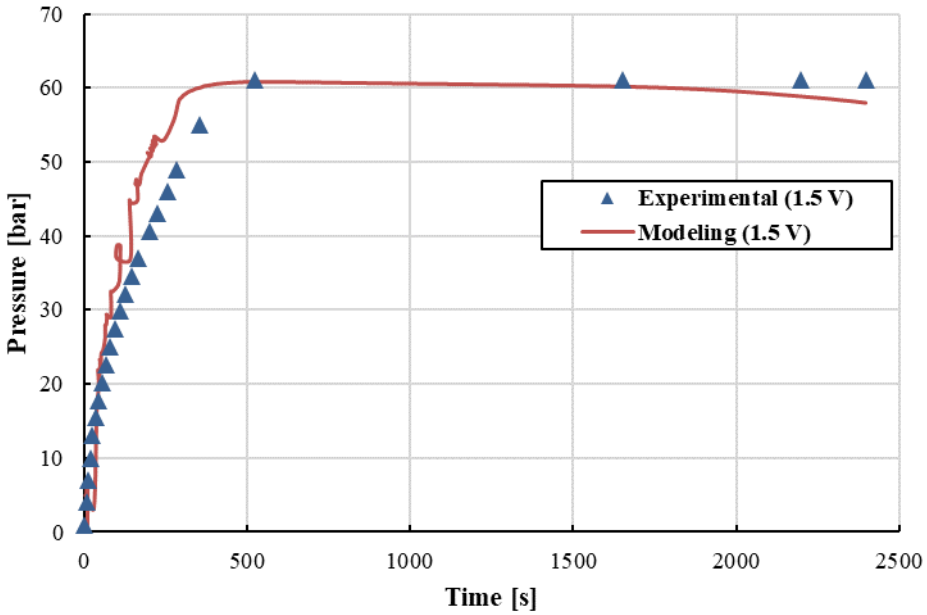

Figure 4. 27 Change of cathode pressure with time at a constant cell voltage of 1.5 V

4.4.4 Investigation of Efficiency of ECHC Cell at Different Cell Voltages

The changes in voltage, molar flow rate and cell efficiency values of the ECHC cell over time were examined using Equations 4.24, 2.25 and 4.26. In Equation 4.26, which is the mathematical expression of the efficiency of the ECHC cell, the cell voltage begins from 0 due to the equality of pressures at both the anode and cathode, and at atmospheric pressure when the ECHC cell starts operating. When the results given for 0.1 V constant cell voltage in Figure 75 are examined, it is determined that the cell efficiency increases with the increase in H_2 molar flow rate. As the cell voltage reaches equilibrium, the forward H_2 molar flow rate stabilizes, and the cathode pressure reaches equilibrium. As the pressure stabilized, the voltage efficiency increased to 45% and reached equilibrium. It was observed that back diffusion had no effect due to the lack of anode and cathode pressure difference at the beginning and the molar flow rate efficiency started from 100% and decreased to 10% with time. The reason for this is that the backward H_2 molar flow rate increases due to the pressure difference. A

decrease in molar flow rate efficiency was observed because the increase in the backward H_2 molar flow rate decreased the net H_2 molar flow rate. It was determined that the cell efficiency obtained by multiplying the molar flow rate and cell efficiency values reached 25% but then decreased due to the voltage efficiency reaching equilibrium and the molar flow rate efficiency decreasing due to the back diffusion effect.

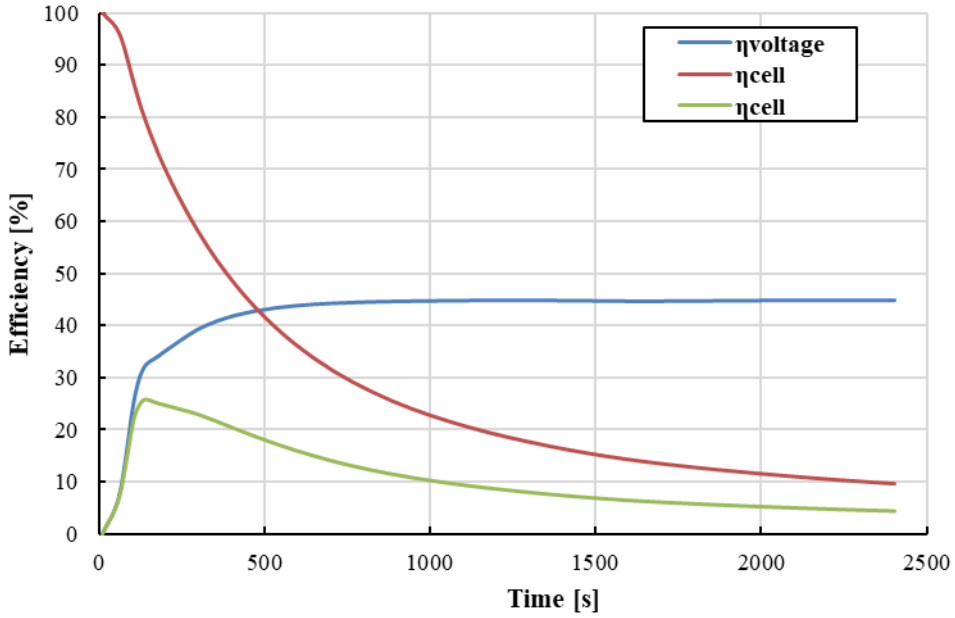

Figure 4. 28 Variation of ECHC cell current, voltage, and cell efficiency with time at a constant cell voltage of 0.1 V

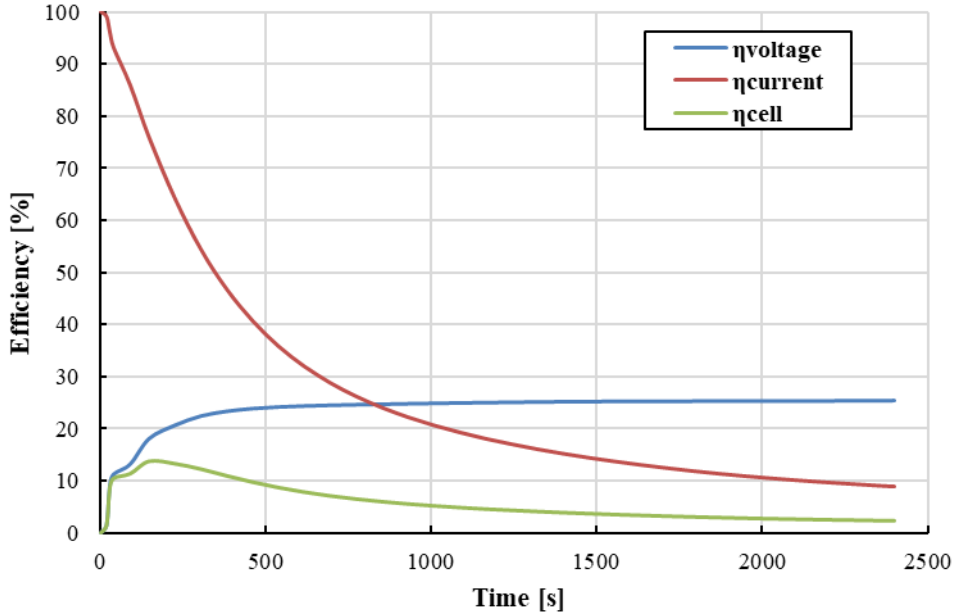

Figure 4. 29 Variation of ECHC cell current, voltage, and cell efficiency with time at a constant cell voltage of 0.2 V

Figure 4.29 covers the voltage, molar flow rate and cell efficiency results obtained at a constant cell voltage of 0.2 V. Upon reviewing the results, it was observed that the voltage efficiency decreased to 25% as the cell voltage was increased to 0.2 V.

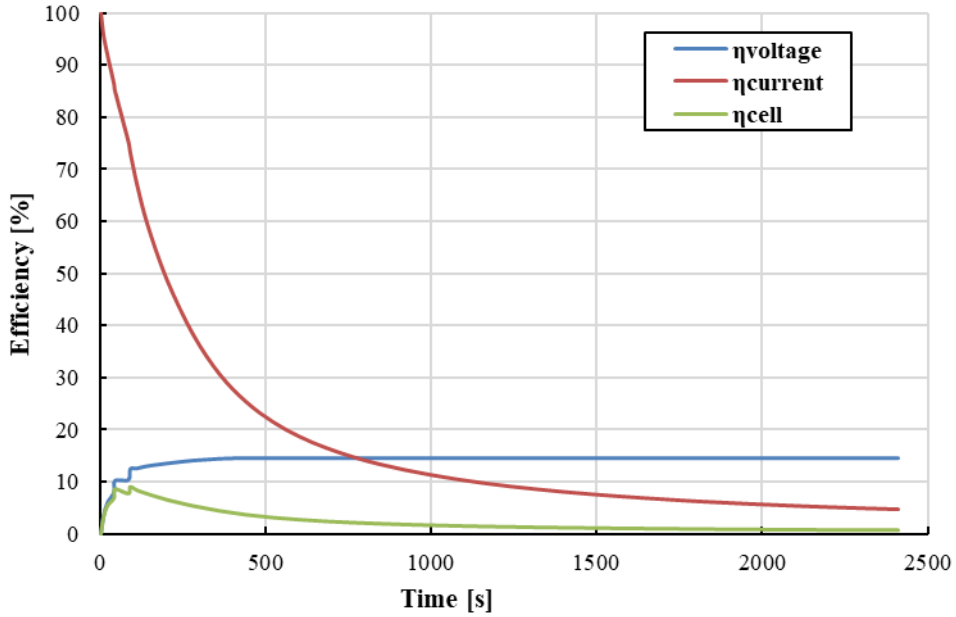

Figure 4. 30 Variation of ECHC cell current, voltage, and cell efficiency with time at a constant cell voltage of 0.4 V

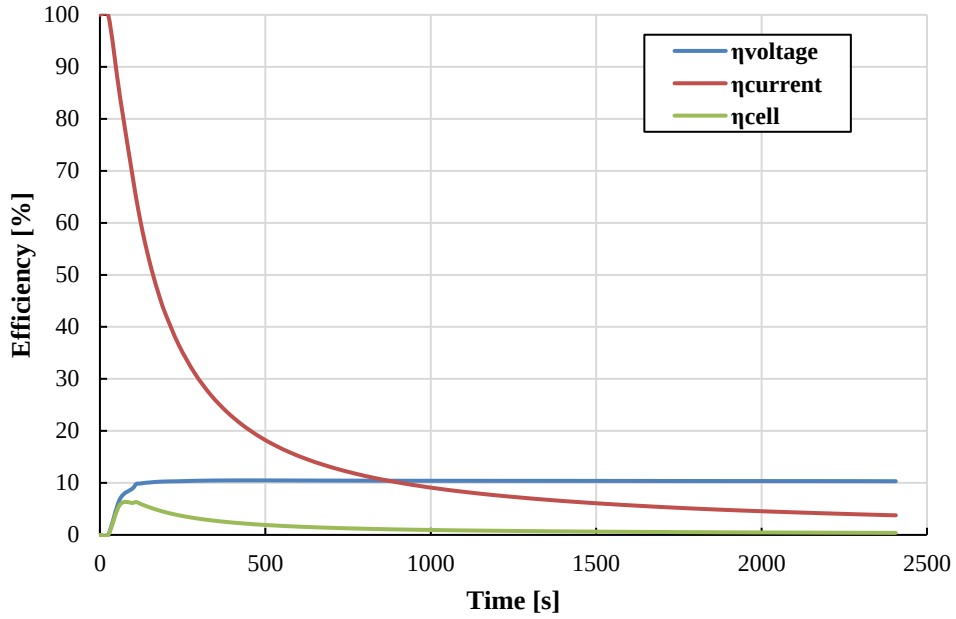

Figure 4. 31 Variation of ECHC cell current, voltage, and cell efficiency with time at a constant cell voltage of 0.6 V

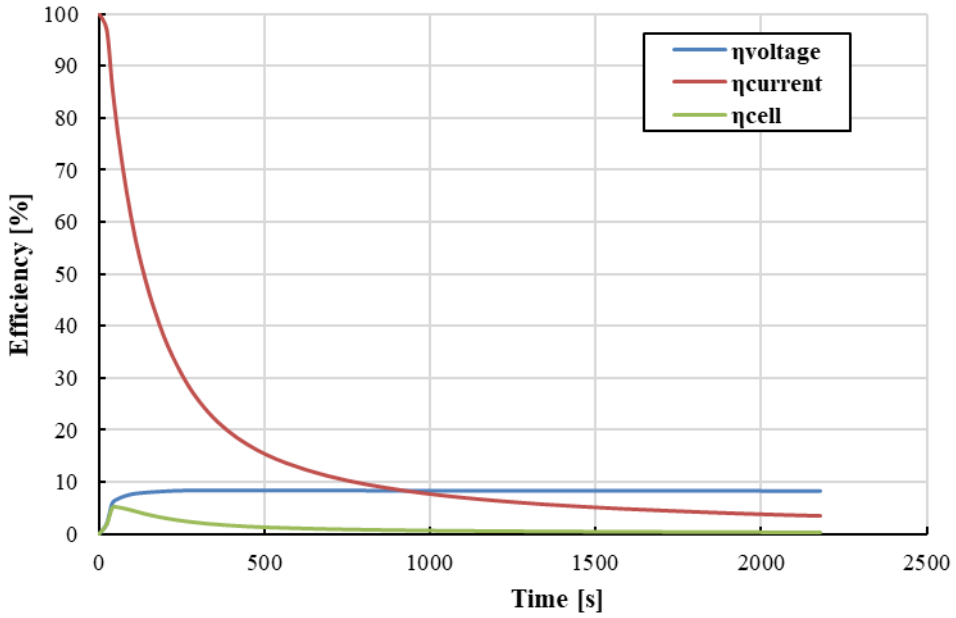

Figure 4. 32 Variation of ECHC cell current, voltage, and cell efficiency with time at a constant cell voltage of 0.8 V

The variation of ECHC cell current, voltage, and cell efficiency with time for constant cell voltages of 0.4 V, 0.6 V, 0.8 V, 1 V and 1.5 V is shown in Figure 4.30, Figure 4.31, Figure 4.32, Figure 4.33 and Figure 4.34, respectively.

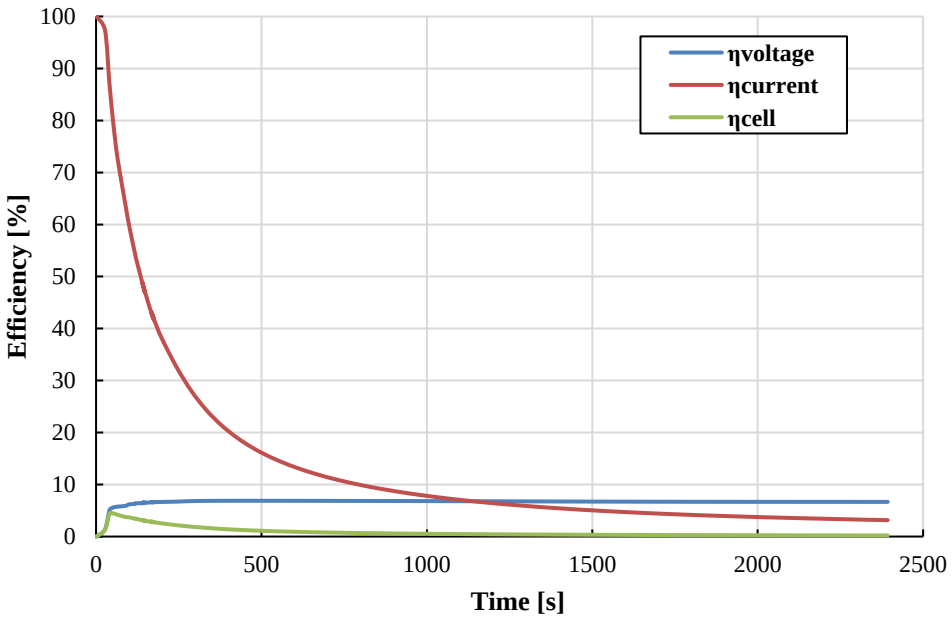

Figure 4. 33 Variation of ECHC cell current, voltage, and cell efficiency with time at a constant cell voltage of 1 V

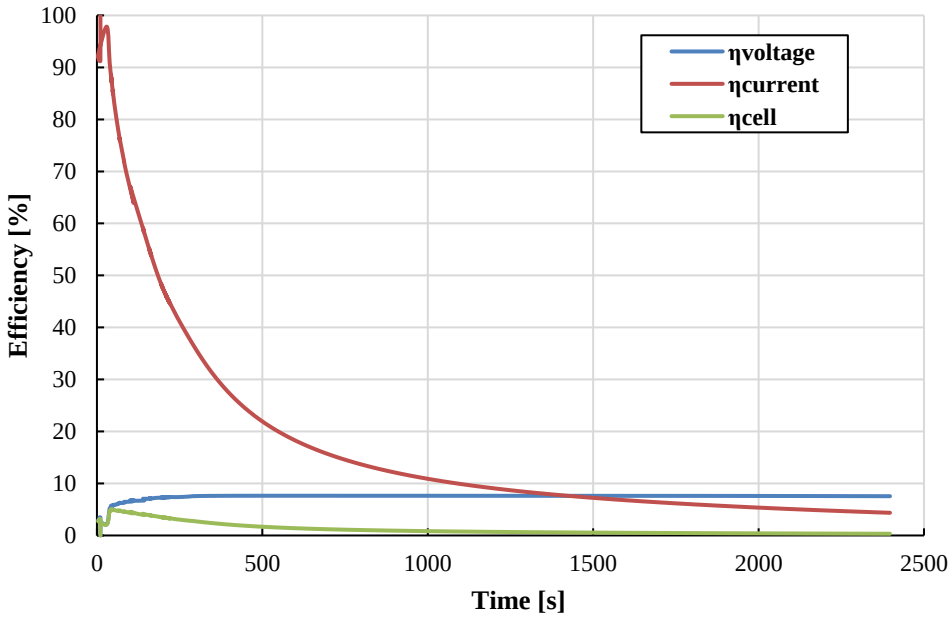

Figure 4. 34 Variation of ECHC cell current, voltage, and cell efficiency with time at a constant cell voltage of 1.5 V

4.5 Investigation of the 5-cell Stack through Modeling

In section 3.1.3.1, a model of a series-connected stack consisting of five cells is systematically developed. This involved the detailed creation of control volumes to establish a comprehensive balance for the entry and exit of gases. The aim was to calculate the pressure value reached by the cell according to the inlet and outlet net flux value thus created. In the 5-cell ECHC stack, 60 bar compression pressure was reached in 400 seconds. Figure 4.35 represents the pressure curve obtained in the stack level model at a constant cell voltage of 7.5 V and verified by experimental data.

From the results obtained, it was determined that the difference between the experimental and modeling results for both single-cell and five-cell ECHC stacks was within ±5% at most.

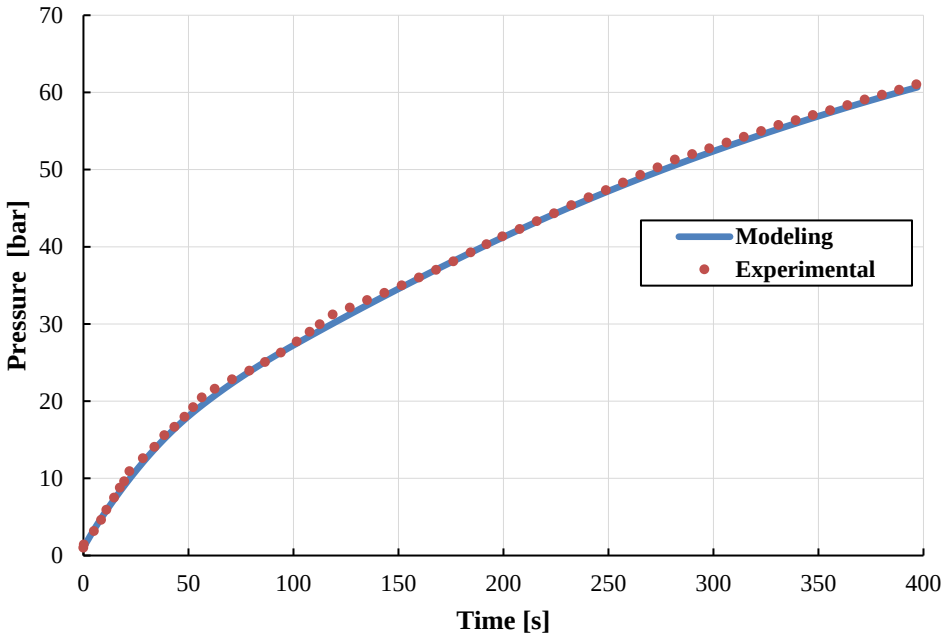

Figure 4. 35 Variation of ECHC stack level cell pressure with time at a constant cell voltage of 7.5 V and comparison with experimental data

4.6 Characterizing the ECHC Cell's Polarization Curve through Parameter Calibration with the PSO Algorithm

Figure 4.36 shows the current drawn by the cell from the power supply at a constant voltage of 0.1 V. As can be seen from the figure, it was seen that the current value reached equilibrium and remained constant after a certain period. This value means the current needed by the cell to operate at that voltage value. This process was applied for 0.2 V, 0.4 V 0.6 V 0.8 V, and 1 V. Then, the obtained values were combined to form the polarization curve of the cell. The calculation of parameters to be used in the mathematical model using the PSO algorithm was calculated by defining the upper and lower limit values as shown in Table 3.2. Figure 4.37 represents the experimental and modeling results.

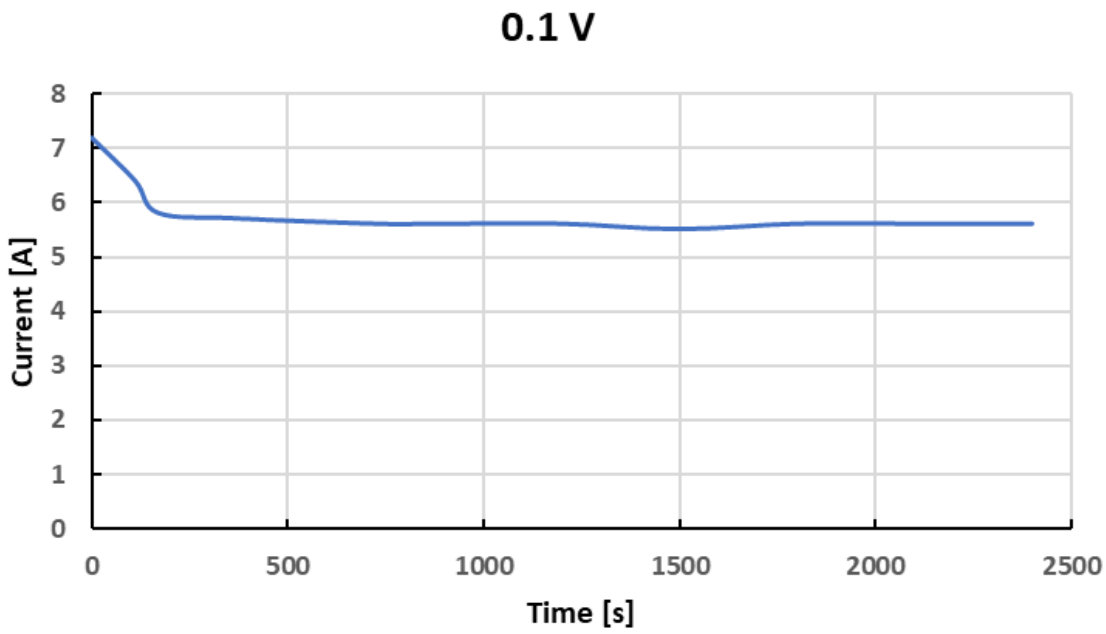

Figure 4. 36 The current drawn by the cell under constant 0.1 V

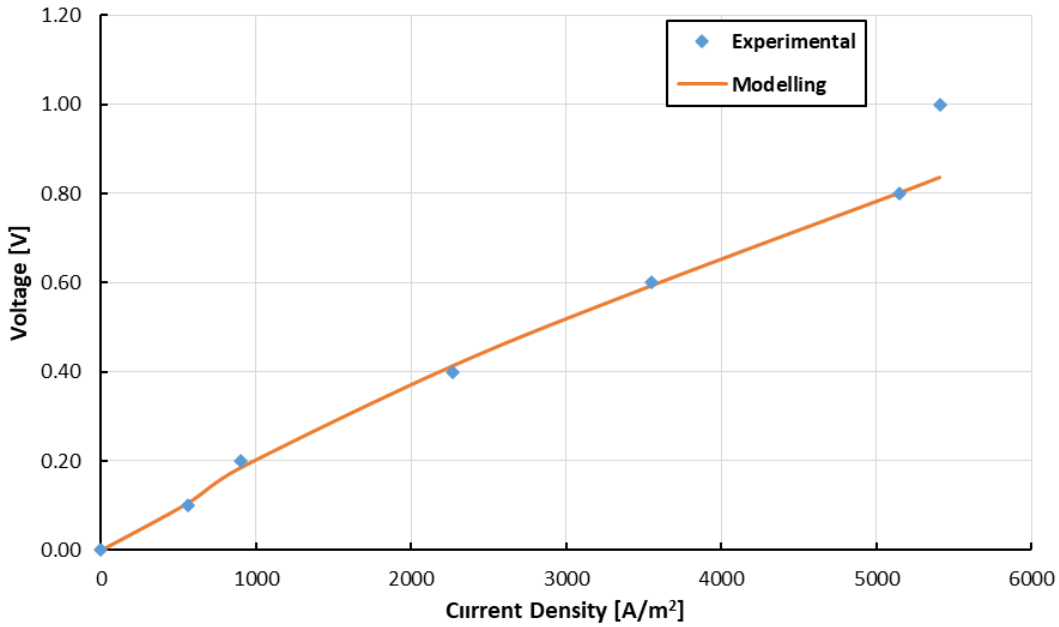

Figure 4. 37 Current voltage curve of the cell

It has been seen that the result obtained with the PSO algorithm, which is used to determine the parameters of the created chemical model, is very well matched with the experimental studies. It was observed that there was a deviation of approximately 10% when high current values were increased. This deviation may be due to catalyst poisoning. This error can be minimized by integrating a formula that covers the poisoning effect into the modeling and increasing the number of iterations.

CHAPTER FIVE
CONCLUSIONS

Within the scope of this thesis, semi-empirical mathematical models have been developed to examine the parameters affecting the performance of the PBI membrane-based ECHC cell, which has the ability to both purify and pressurize H_2 in a single device and can operate in the high temperature range (140°C-180°C) and the H_2 compression performance of HT-ECHC under high-temperature operating conditions was investigated by both experimental and modeling studies. Model results have been validated with both literature data and experimental data.

The following points were obtained in this thesis.

- In the first part of the thesis, the performance of the ECHC cell when fed with both pure hydrogen and reformate gas in the range of 140°C-180ºC was examined and i-V curves were created in this context. According to the obtained values, the temperature at which the cell operates most efficiently was determined as 160°C.
- Polarization curves obtained by considering gas mixtures with H_2CO (0.97:0.03) and H_2CO (0.95:0.05) ratios were examined. According to the data obtained, at the same cell voltage value, higher current density was obtained in the case of mixed gas feed with low CO content. It can be said that this is due to the increase in the poisoning rate of catalysts as the amount of CO increases.
- To determine the performance curves of the ECHC cell, forward, backward, and net hydrogen molar flow rates at constant cell voltages were calculated and presented graphically for a single-cell ECHC created in MATLAB software. The pressure value and the membrane gas permeability coefficient increased with the increase in cell voltage. At a constant 1.5 V cell voltage, the highest value of 60 bar pressure has been reached and the increase in cell voltage caused a decrease in current and voltage efficiency.

- It was determined that the 5-cell, 7.5 V constant voltage ECHC cell (the voltage of each cell is 1.5 V because it is connected in series) reached the compression pressure of 60 bar in a shorter time than the single-cell case.
- It was found that, for both single-cell and five-cell ECHC stacks, the variation between the modeling and experimental findings was, at most, ±5%.

ECHC systems are efficient devices that offer both purification and compression functionalities within a singular device. Due to its quiet operation, clean appearance, and lack of additional maintenance expenditures, it has the potential to take a significant role in the industry going forward. It is expected that the data and modeling techniques presented in this thesis will be an important guiding study for researchers working in this field in the future.

REFERENCES

Amil, C., & Yılmazoğlu, M. Z. (2022). The importance of hydrogen for energy diversity of Turkey's energy production: 2030 projection. *International Journal of Hydrogen Energy*, *47*(45), 19935–19946. https://doi.org/10.1016/j.ijhydene.2022.03.274

Ball, M., & Wietschel, M. (2009). The future of hydrogen - opportunities and challenges. *International Journal of Hydrogen Energy*, *34*(2), 615–627. https://doi.org/10.1016/j.ijhydene.2008.11.014

Bampaou, M., Panopoulos, K. D., Papadopoulos, A. I., Seferlis, P., & Voutetakis, S. (2018). An electrochemical hydrogen compression model. *Chemical Engineering Transactions*, *70*(1), 1213–1218. https://doi.org/10.3303/CET1870203

Bulanık Durmuş, G. N., Kuzu, C., Devrim, Y., & Colpan, C. O. (2024). Experimental and modeling studies of a high-temperature electrochemical hydrogen compressor. *International Journal of Hydrogen Energy*, *51*, 290–301. https://doi.org/10.1016/j.ijhydene.2023.04.235

Cao, Q. (2017). Modelling of High Temperature Polymer Electrolyte Fuel Cells Modellierung von Hochtemperatur-Polymerelektrolyt- Brennstoffzellen. *Thesis*.

Chandan, A., Hattenberger, M., El-Kharouf, A., Du, S., Dhir, A., Self, V., Pollet, B. G., Ingram, A., & Bujalski, W. (2013). High temperature (HT) polymer electrolyte membrane fuel cells (PEMFC)-A review. *Journal of Power Sources*, *231*, 264–278. https://doi.org/10.1016/j.jpowsour.2012.11.126

Cheddie, D., & Munroe, N. (2006). Mathematical model of a PEMFC using a PBI membrane. *Energy Conversion and Management*, *47*(11–12), 1490–1504. https://doi.org/10.1016/j.enconman.2005.08.002

Chouhan, A., Aryal, U. R., Bahar, B., & Prasad, A. K. (2020). Analysis of an electrochemical compressor stack. *International Journal of Hydrogen Energy*, *45*(56), 31452–31465. https://doi.org/10.1016/j.ijhydene.2020.08.164

Chouhan, A., Bahar, B., & Prasad, A. K. (2020). Effect of back-diffusion on the performance of an electrochemical hydrogen compressor. *International Journal of Hydrogen Energy*, *45*(19), 10991–10999. https://doi.org/10.1016/j.ijhydene.2020.02.048

Dale, N. V., Mann, M. D., Salehfar, H., Dhirde, A. M., & Han, T. (2007, March). Modeling and analysis of electrochemical hydrogen compression. In Proceedings of the NHA Annual Hydrogen Conference, Sacramento Convention Center, Sacramento, CA, USA (Vol. 30).

Dincer, I. (2020). Covid-19 coronavirus: Closing carbon age, but opening hydrogen age. *International Journal of Energy Research*, *44*(8), 6093–6097.

https://doi.org/10.1002/er.5569

Dincer, I., & Acar, C. (2018). Smart energy solutions with hydrogen options. *International Journal of Hydrogen Energy*, *43*(18), 8579–8599. https://doi.org/10.1016/j.ijhydene.2018.03.120

Disli, T., Çetinkaya, S. A., Ezan, M. A., & Colpan, C. O. (2023). Numerical investigations on the absorption of a metal hydride hydrogen storage tank based on various thermal management strategies. *International Journal of Hydrogen Energy*, *xxxx*. https://doi.org/10.1016/j.ijhydene.2023.07.122

Dornheim, M., Baetcke, L., Akiba, E., Ares, J. R., Autrey, T., Barale, J., Baricco, M., Brooks, K., Chalkiadakis, N., Charbonnier, V., Christensen, S., Bellosta Von Colbe, J., Costamagna, M., Dematteis, E., Fernandez, J. F., Gennett, T., Grant, D., Heo, T. W., Hirscher, M., … Zoulias, E. (2022). Research and development of hydrogen carrier based solutions for hydrogen compression and storage. *Progress in Energy*, *4*(4). https://doi.org/10.1088/2516-1083/ac7cb7

Durmuş, G. N. B. (2023). *YEAR*. *June*.

Durmus, G. N. B., Colpan, C. O., & Devrim, Y. (2021). A review on the development of the electrochemical hydrogen compressors. *Journal of Power Sources*, *494*(February), 229743. https://doi.org/10.1016/j.jpowsour.2021.229743

Eberhart, R., & Kennedy, J. (1995). New optimizer using particle swarm theory. *Proceedings of the International Symposium on Micro Machine and Human Science*, 39–43. https://doi.org/10.1109/mhs.1995.494215

Freitas, D., Lopes, L. G., & Morgado-Dias, F. (2020). Particle Swarm Optimisation: A historical review up to the current developments. *Entropy*, *22*(3), 1–36. https://doi.org/10.3390/E22030362

Kulikovsky, A. A. (2019). *Analytical modelling of fuel cells*. Elsevier.

Leng, Y., Ming, P., Yang, D., & Zhang, C. *(2020). Stainless steel bipolar plates for proton exchange membrane fuel cells: Materials, flow channel design and forming processes. Journal of Power Sources, 451, 227783.*.

Marciuš, D., Kovač, A., & Firak, M. (2022). Electrochemical hydrogen compressor: Recent progress and challenges. *International Journal of Hydrogen Energy*, *47*(57), 24179–24193. https://doi.org/10.1016/j.ijhydene.2022.04.134

Mench, M. M. (2008). *Fuel Cell Engines*.

Nalbant, Y., Colpan, C. O., & Devrim, Y. (2018). Development of a one-dimensional and semi-empirical model for a high temperature proton exchange membrane fuel cell. *International Journal of Hydrogen Energy*, *43*(11), 5939–5950. https://doi.org/10.1016/j.ijhydene.2017.10.148

Neyerlin, K. C., Singh, A., & Chu, D. (2008). Kinetic characterization of a Pt-Ni/C catalyst with a phosphoric acid doped PBI membrane in a proton exchange membrane fuel cell. *Journal of Power Sources*, *176*(1), 112–117. https://doi.org/10.1016/j.jpowsour.2007.10.030

Nordio, M., Rizzi, F., Manzolini, G., Mulder, M., Raymakers, L., Van Sint Annaland, M., & Gallucci, F. (2019). Experimental and modelling study of an electrochemical hydrogen compressor. *Chemical Engineering Journal*, *369*, 432–442. https://doi.org/10.1016/j.cej.2019.03.106

Özdemir, Y., Üregen, N., & Devrim, Y. (2017). Polybenzimidazole based nanocomposite membranes with enhanced proton conductivity for high temperature PEM fuel cells. *International Journal of Hydrogen Energy*, *42*(4), 2648–2657. https://doi.org/10.1016/j.ijhydene.2016.04.132

Rhandi, M., Trégaro, M., Druart, F., Deseure, J., & Chatenet, M. (2020). Electrochemical hydrogen compression and purification versus competing technologies: Part I. Pros and cons. Chinese Journal of Catalysis, 41(5), 756-769.

Rohland, B., Eberle, K., Stroè, R., Scholta, J., & Garche, J. (n.d.). *Electrochemical hydrogen compressor*.

Sadaghiani, M. S., & Mehrpooya, M. (2017). Introducing and energy analysis of a novel cryogenic hydrogen liquefaction process configuration. *International Journal of Hydrogen Energy*, *42*(9), 6033–6050. https://doi.org/10.1016/j.ijhydene.2017.01.136

Sdanghi, G., Maranzana, G., Celzard, A., & Fierro, V. (2019). Review of the current technologies and performances of hydrogen compression for stationary and automotive applications. *Renewable and Sustainable Energy Reviews*, *102*(May 2018), 150–170. https://doi.org/10.1016/j.rser.2018.11.028

Sdanghi, G., Maranzana, G., Celzard, A., & Fierro, V. (2020). Towards non-mechanical hybrid hydrogen compression for decentralized hydrogen facilities. *Energies*, *13*(12). https://doi.org/10.3390/en13123145

Ströbel, R., Oszcipok, M., Fasil, M., Rohland, B., Jörissen, L., & Garche, J. (2002). The compression of hydrogen in an electrochemical cell based on a PE fuel cell design. Journal of power sources, 105(2), 208-215.

Tahan, M. R. (2022). Recent advances in hydrogen compressors for use in large-scale renewable energy integration. *International Journal of Hydrogen Energy*, *47*(83), 35275–35292. https://doi.org/10.1016/j.ijhydene.2022.08.128

Toghyani, S., Afshari, E., & Baniasadi, E. (2020). Parametric study of a proton exchange membrane compressor for electrochemical hydrogen storage using numerical assessment. *Journal of Energy Storage*, *30*(March), 101469.

https://doi.org/10.1016/j.est.2020.101469

Yelegen, N. (2014). Elektrokimyasal hidrojen kompresör yığını geliştirilmesi ve karakterizasyonu (Master's thesis, Niğde Üniversitesi)

Zou, J., Han, N., Yan, J., Feng, Q., Wang, Y., Zhao, Z., Fan, J., Zeng, L., Li, H., & Wang, H. (2020). Electrochemical Compression Technologies for High-Pressure Hydrogen: Current Status, Challenges and Perspective. *Electrochemical Energy Reviews*, *3*(4), 690–729. https://doi.org/10.1007/s41918-020-00077-0